Advanced Research for Development of Highly Sensitive Detection Methods and Antibody Therapeutics using Monoclonal Antibody Discovery and Biochemical Methods

January 2024

Shuuichi MIYAKAWA

Advanced Research for Development of Highly Sensitive Detection Methods and Antibody Therapeutics using Monoclonal Antibody Discovery and Biochemical Methods

A Dissertation Submitted to
the Graduate School of Science and Technology,
University of Tsukuba
in Partial Fulfillment of Requirements
for the Degree of Doctor of Philosophy in Science
Doctoral Program in Biology,
Degree Programs in Life and Earth Sciences

Shuuichi MIYAKAWA

Table of contents

Abstract

Antibodies are proteins that play a crucial role in the immune defense mechanism of living organisms. They recognize and neutralize specific foreign substances or proteins (antigens) and eliminate them from the body. Monoclonal antibodies, obtained from a single antibody-producing B cell, have revolutionized the field of medicine and research since their development in 1975 by César Milstein and Georges Köhler. The hybridoma technology used to produce monoclonal antibodies has enabled the production of large quantities of highly specific and homogeneous antibodies, which have contributed significantly to the advancement of life sciences. Monoclonal antibodies are widely used in the biotechnology industry, for the identification and functional analysis of specific proteins, the identification of cell surface markers, and the detection of biomarkers in disease diagnosis and treatment. They are also important therapeutic options for the treatment of cancer and autoimmune diseases, forming a significant market for biopharmaceuticals.

In this study, I investigated the method of producing monoclonal antibodies to low molecular weight compounds, which are generally considered difficult in aspect of specificity and strength of binding, and succeeded in establishing a system to quantify and clarify the dynamics of cGAMP, an important second messenger in cells and tissue.

In addition, I explored the therapeutic potential of sortilin1 (SORT1), a clearance receptor of Progranulin, by generating and characterizing monoclonal antibodies against it, which contribute to cure of the neurodegenerative disease, frontotemporal dementia (FTD), characterized by the selective and progressive degeneration of the frontotemporal lobe.

Thus, my study has largely contributed to the methodology for increasing the number of target molecules of monoclonal antibodies, especially low molecular weight compounds, and to the development of antibody-based therapeutics for the treatment of diseases.

Abbreviations

AGS	Aicardi–Goutières syndrome
AMC	anti-mouse Fc
BBB	blood-brain barrier
BCA	bicinchoninic acid
BLI	biolayer interferometry
cGAMP	cyclic GMP-AMP
cGAS	cyclic GMP-AMP synthase
CSF	cerebrospinal fluid
DIV	days in vitro
dsDNA	double-stranded DNA
EDC	1-ethyl-3-(3-dimethylaminopropyl)carbodiimide hydrochloride
ELISA	enzyme-linked immunosorbent assay
FCM	flow cytometry
FcRn	neonatal Fc receptor
FP	fluorescence polarization
FTD	frontotemporal dementia
ICC	immunocytochemical
IEC	ion-exchange chromatography
IFN	interferon
IHC	immunohistochemistry
IRF3	interferon regulatory factor-3
ISF	interstitial fluid
KLH	keyhole limpet hemocyanin
KO	knockout
LDL	low-density lipoprotein
mAb	monoclonal antibody
mc	mariculture
MEM	minimum Eagle medium
NTS	neurotensin
OD	optical density
OD450	optical density at 450 nm
PBS	phosphate-buffered saline
PBST	PBS containing 0.05% Tween-20
PFA	paraformaldehyde

PGRN	progranulin
RI	radioisotope
SD	standard deviation
SLE	systemic lupus erythematosus
SORT1	sortilin1
SPR	surface plasmon resonance
STING	stimulator of interferon genes
TBK1	TANK-binding kinase 1
TBS	Tris-buffered saline
TBST	Tris-buffered saline containing 0.1% Tween-20
TLC	thin-layer chromatography
TREX1	3' repair exonuclease 1
TR-FRET	time-resolved fluorescence energy transfer
VLDL	very low-density lipoprotein
WT	wild-type

General introduction

Antibodies are proteins that function in the body's immune defense mechanisms. Antibodies are mainly responsible for humoral immunity in adaptive immunity, which recognizes specific foreign substances and proteins, neutralizes their functions and eliminates them from the body. They are produced by specialized cells called B-lymphocytes that recognize and bind to specific antigens on the surface of pathogens. This triggers a series of events that lead to the destruction of pathogens and activation of other immune cells. Antibodies are also involved in the recognition and removal of abnormal or damaged cells, such as cancer cells.

Antibodies are usually present *in vivo* as polyclonal antibodies that contain multiple clones. In 1975, Cesar Milstein and Georges Köhler were the first to develop a method for producing monoclonal antibodies (Köhler and Milstein, 1975), for which they were awarded the Nobel Prize in Physiology or Medicine in 1984. The hybridoma method used in this development is an innovative technology. It is a method of injecting antigens into animals such as mice to induce an immune response and fusing antibody-producing B-lymphocytes with tumor cells. Next, hybridoma cells with both the ability of immune cells to produce antigen-specific antibodies and the ability to proliferate immortalized tumor cells are selected. This has made it possible to produce monoclonal antibodies in large quantities, which has led to various innovations in medicine and research.

Its specificity and versatility make monoclonal antibodies a powerful tool in biomedical research and clinical practice, with applications ranging from basic science to diagnosis and treatment. The use of monoclonal antibodies greatly contributes to the development of life science through functional analysis of specific proteins and identification of cell surface markers. These characters are widely used in the biotechnology industry such in the detection of biomarkers in the diagnosis or treatment of diseases. In drug development, monoclonal antibodies have become an important therapeutic option, forming a large market for biopharmaceuticals used to treat cancer and autoimmune diseases. The antibody generation technology enables us to supply large amount of antibodies of stable quality over a long period of time with high specificity and binding affinity for the antigen. This property has led to the application of monoclonal antibodies for the detection and quantification of specific molecules and therapeutic agents.

Both affinity and specificity in monoclonal antibodies are key issues when using antibodies in scientific research. Affinity refers to the strength of the bond between an antibody and its target antigen. High-affinity antibodies bind more tightly to antigens, which can improve the sensitivity and accuracy of assays and experiments. However, if the affinity is too high, the antibody can bind to other molecules that are structurally similar to the antigen,

causing false positives or cross-reactivity. On the other hand, if the affinity is too low, the antibody may not be able to detect the antigen in low concentrations or complex samples. Specificity refers to an antibody's ability to recognize and bind only to the target antigen of interest without cross-reacting with other molecules. Highly specific antibodies minimize the risk of false positives and improve confidence in results. However, achieving high specificity can be challenging, especially when dealing with complex samples containing many different molecules that may share structural similarities with the antigen of interest. Cross-reactivity also needs to be evaluated. Even if an antibody is specific to the target antigen of interest, it can cross-react with other molecules that are structurally similar or present in the sample. This can lead to false positives or interference with the detection of the target antigen. Thus, it is important to carefully select and validate antibodies for each specific application using appropriate controls and assays to assess their affinity and specificity. This helps to ensure the accuracy and reproducibility of scientific research results. However, when the specificity of these antibodies has not been sufficiently verified and functionally evaluated, appropriate results may not always be obtained. Given the widespread use of antibodies, this is a very important issue and can lead to significant losses in scientific field as well as therapeutic industry. In this study, I aimed to establish a detection system for highly sensitive quantification of cGAMP and applied anti-SORT1 antibody to antibody drug through the novel antibody discovery, their functional analysis, and biochemical evaluation.

Chapter 1

Development of novel highly sensitive methods to detect endogenous cGAMP in cells and tissue

Abstract

Intracellular DNA triggers interferon release during the innate immune response. Cyclic GMP-AMP synthase (cGAS) senses intracellular double-stranded DNA not only in response to viral infection but also under autoimmune conditions. Measuring the levels of cyclic GMP-AMP (cGAMP) as a second messenger of cGAS activation is important to elucidate the physiological and pathological roles of cGAS. Therefore, I generated monoclonal antibodies against cGAMP using hybridoma technology to test antibody specificity and establish methods to detect intracellular cGAMP. The resulting cGAMP-specific antibody enabled the development of a time-resolved fluorescence energy transfer assay with a quantifiable range of 0.1 nM to 100 nM cGAMP. Using this assay, I was able to detect cellular and tissue cGAMP and confirmed that the cGAMP antibody successfully targeted intracellular cGAMP through immunocytochemical analyses. These results demonstrated that the cGAMP antibody is a powerful tool that allows determining cGAS involvement in autoimmunity and disease pathology at the cell and tissue levels.

Introduction

Cyclic GMP-AMP synthase (cGAS) catalyzes the generation of cyclic GMP-AMP (cGAMP) from ATP and GTP (Gao et al., 2013; Sun et al., 2013) and binds cytoplasmic double-stranded DNA (dsDNA) from viral origin, which results in cGAS activation and triggers an immune reaction (Civril et al., 2013; Wu et al., 2013). cGAMP produced by cGAS activates stimulator of interferon (IFN) genes (STING), which induces the expression of inflammatory mediators, including type I IFNs, via the TANK-binding kinase-1 (TBK1)/IFN-regulatory factor-3 (IRF3) signaling pathway (Ishikawa et al., 2009; Tanaka and Chen, 2012; Kato et al., 2013) and sequentially induces the production of multiple IFN-stimulated genes involved in disruption of the viral life cycle (Ishikawa et al., 2009; Li et al., 2013b). These findings indicate that the cGAS–cGAMP–STING axis acts as a key contributor to the antiviral response.

Additionally, recent studies highlighted the involvement of this pathway in the pathology of autoimmune diseases. Aicardi–Goutières syndrome (AGS) is a rare, early-onset autoimmune disease in which chronic expression of type I IFN results in lupus-like systemic autoimmunity (Crow and Manel, 2015; Rodero and Crow, 2016). AGS is caused by mutations in *3' repair exonuclease 1 (TREX1)*, *RNASEH2A*, *RNASEH2B*, *RNASEH2C*, *SAM-domain- and HD-domain-containing protein 1*, *adenosine deaminase 1*, or *IFN induced with helicase C domain 1,* each of which is involved in nucleic acid pathways or nucleotide metabolism (Livingston and Crow, 2016), suggesting that an aberrant regulation of nucleic acids induces the chronic inflammation observed in AGS patients.

Mice deficient in *Trex1*, a cellular DNA exonuclease, used as preclinical models of AGS, revealed the involvement of cGAS in this autoimmune disease, showing that cGAS deficiency completely attenuated the lethal, lupus-like autoimmune phenotype observed in *Trex1*-deficient mice (Gao et al., 2015; Gray et al., 2015). These findings suggest that an excessive accumulation of undegraded DNA induces chronic inflammation through cGAS in AGS.

Additionally, cGAS is associated with human systemic lupus erythematosus (SLE) pathology. SLE patients upregulate cGAS and its direct product cGAMP when compared to controls subjects (An et al., 2017). Moreover, serum from SLE patients shows elevated levels of type I IFNs associated with the cGAS and STING pathways. SLE sera had a significantly reduced ability to induce the expression of type I IFN genes in *STING*-knockout cells (Kato et al., 2018). Although a preclinical study demonstrated that mice deficient in *Sting* crossed with the SLE-prone strain MRL. Fas^{lpr} showed aggravated disease manifestations in an *Irf3*-independent manner, suggesting the suppressive functions of *Sting* in systemic autoimmunity (Sharma et al., 2015), evidence in humans strongly suggests the causal role and therapeutic

potential of the cGAS–cGAMP–STING axis in association with autoimmune diseases related to dysfunctional processing of cytoplasmic DNA.

Previous studies described cGAS function as contributing to the antiviral response (Ishikawa et al., 2009; Li et al., 2013b) or autoimmune pathology (An et al., 2017), and several methods have been used to monitor cGAS activity by assessing its downstream signals, including those of cGAMP, TBK1, IRF3, and IFNβ (Sun et al., 2013; Hansen et al., 2014). Although cGAMP is a direct cGAS product, TBK1, IRF3, or IFNβ activation is indirectly promoted by molecules other than cGAS.

Therefore, in this study, I focused on cGAMP detection to assess cGAS activity. Few methods allow detecting cGAMP as an indicator of cGAS activation. Previous studies reported the use of thin-layer chromatography (TLC) plus radioisotope (RI) or ion-exchange chromatography (IEC) to detect cGAMP production in the presence of recombinant cGAS protein (Diner et al., 2013; Gao et al., 2013; Li et al., 2013a). Liquid chromatography-mass spectrometry (LC-MS) was used to measure endogenous cell or tissue cGAMP levels (Ablasser et al., 2013; Sun et al., 2013; Wu et al., 2013; Gao et al., 2015; Gray et al., 2015). Additionally, an RNA aptamer was developed as a cGAMP biosensor (Bose et al., 2016), and a high-throughput cGAS fluorescence-polarization (FP)-based assay was used to identify cGAS inhibitors using recombinant cGAS protein (Hall et al., 2017). Recently, cGAMP enzyme-linked immunosorbent assay (ELISA) was used to detect cellular cGAMP (Gentili et al., 2019). However, these approaches are not readily applicable for drug discovery due to the insufficient throughput of LC-MS-based methods and ELISA, the sensitivity of FP-based assays, or the specificity of an RNA aptamer.

To overcome these limitations, I developed a monoclonal antibody (mAb) specific to cGAMP that allowed us to successfully establish a time-resolved fluorescence resonance energy transfer (TR-FRET) assay with a detection range of 0.1 nM to 100 nM. These results showed that the assay exhibited a high degree of sensitivity and was easily adaptable for high-throughput screening. Moreover, the mAb successfully detected cellular and tissue cGAMP according to the TR-FRET assay and immunocytochemical (ICC) assays. These results promote further in-depth research into the involvement of cGAS in immune function.

Materials and Methods

mAb generation

Keyhole limpet hemocyanin (KLH)-conjugated 2'3'-cGAMP (cGAMP-KLH) was used as an antigen to raise anti-cGAMP antibody levels. cGAMP-KLH was prepared as follows. Mariculture (mc) KLH (2 mg; Thermo Fisher Scientific, Waltham, MA, USA) was reconstituted in 200 µL of distilled water, and 5 µmol of cGAMP-NH_2 (BioLog, Hayward, CA, USA) was dissolved in 500 µL 1-ethyl-3-(3-dimethylaminopropyl)carbodiimide hydrochloride (EDC) conjugation buffer [0.1 M MES, 0.9 M NaCl (pH 4.7)]. The mcKLH and cGAMP-NH_2 solutions were combined and used to dissolve 10 mg of EDC. After a 2-h incubation at room temperature, the cGAMP-KLH solution was dialyzed in 1 L of phosphate-buffered saline (PBS) for 18 h.

Ten CD2F1/Crlj mice (10-weeks old, female; CLEA Japan, Inc., Tokyo, Japan) were intraperitoneally injected with 100 µg of anti-mCD25 antibody (BioXCell, West Lebanon, NH, USA). After 2 days, the mice were injected subcutaneously into the hock with 20 µg of cGAMP-KLH emulsified with TiterMax Gold adjuvant (TiterMax, Norcross, GA, USA) as part of the first immunization. For the second through the seventh immunizations, mice were injected subcutaneously into the hock with 12 µg of cGAMP-KLH with ODN-1826 (InvivoGen, San Diego, CA, USA) and alum adjuvant twice weekly. After the fifth and seventh immunizations, blood was collected from the tail vein of each mouse, and the plasma antibody titer was tested using an in-house cGAMP ELISA. Briefly, NeutrAvidin (Thermo Fisher Scientific) was used to coat a 96-well plate, and cGAMP-Biotin (BioLog) was bound to the coated NeutrAvidin. Diluted plasma reacted with the plate-bound cGAMP, and cGAMP-reactive IgG was detected using a horseradish peroxidase-conjugated anti-mouse IgG antibody (Jackson ImmunoResearch Laboratories, Inc., West Grove, PA, USA) and SureBlue/TMB peroxidase substrate (SeraCare Life Sciences, Milford, MA, USA). The reaction was stopped by adding H_2SO_4, and the optical density at 450 nm (OD_{450}) was measured using a SpectraMax 340PC384 plate reader (Molecular Devices, Sunnyvale, CA, USA).

Four mice showing high antibody titers were intraperitoneally injected with 20 µg of cGAMP-KLH as the final booster 7 days after the seventh immunization. After 4 days, lymphocytes were isolated from the popliteal lymph nodes of the immunized mice and mixed with P3U1 mouse myeloma cells (ATCC, Manassas, VA, USA) at a 1:1 ratio and subjected to electrofusion using a Legacy ECM 2001 Electro cell fusion and electroporation system (BTX, Holliston, MA, USA) to generate hybridomas.

Hybridoma selection and cloning were performed using ClonaCel-HY Medium D

methylcellulose-based semi-solid medium (STEMCELL Technologies, Vancouver, Canada). Isolated clonal hybridomas were transferred from the semi-solid medium into individual wells of 96-well cell-culture plates containing ClonaCel-HY Medium E (STEMCELL Technologies) using the ClonePix system (Molecular Devices). After 10 days, hybridoma-culture supernatants were screened using in house cGAMP AlphaScreen assay. Briefly, Streptavidin Donor beads (PerkinElmer, Waltham, MA, USA) and anti-mouse IgG-conjugated AlphaScreen Acceptor beads (PerkinElmer) were mixed with cGAMP-Biotin and diluted hybridoma supernatant in 384-well plates with or without a competitor molecule (cGAMP, cAMP, or cGMP) (BioLog). After a 1-h incubation, the Alpha intensity was measured using an Enspire Alpha plate reader (PerkinElmer). Selected hybridomas were expanded in antibody expression medium comprising a mixture of Iscove's modified Eagle medium (MEM; Wako Pure Chemical Industries, Ltd., Osaka, Japan) and Ham's F-12 nutrient medium (Wako Pure Chemical Industries, Ltd.) containing MEM non-essential amino acid solution (Wako Pure Chemical Industries, Ltd.), sodium pyruvate (Wako Pure Chemical Industries, Ltd.), L-alanyl-L-glutamine (Wako Pure Chemical Industries, Ltd.), penicillin and streptomycin (Wako Pure Chemical Industries, Ltd.), at the concentrations indicated in the instruction manual for each reagent, and 10% ultra-low IgG fetal bovine serum (Thermo Fisher Scientific). Anti-cGAMP antibodies were then purified from the culture supernatant using protein A sepharose (GE Healthcare, Pittsburgh, PA, USA). The authors will provide the purified anti-cGAMP antibody #23 upon request for research use only.

Determination of antibody affinity

The kinetic analysis of the affinity of cGAMP to the antibody was performed by surface plasmon resonance (SPR) using a Proteon XPR36 system (Bio-Rad, Hercules, CA, USA). Briefly, purified anti-cGAMP antibody #23 was immobilized on a GLM sensor chip (Bio-Rad) using an amine-coupling kit (Bio-Rad). Serially diluted cGAMP was injected as an analyte, and the sensorgram was analyzed using a 1:1 Langmuir fitting model.

Determination of antibody specificity

Streptavidin Donor beads and anti-mouse IgG-conjugated AlphaScreen Acceptor beads (PerkinElmer) were mixed with 1 nM cGAMP-Biotin and 100 pM anti-cGAMP antibody #23 in the presence of various concentrations of 2'2'-cGAMP, 3'3'-cGAMP, c-di-GMP, c-di-AMP, cGMP, or cAMP (BioLog) in 384-well plates. After a 1-h incubation, the Alpha intensity was measured using an Enspire Alpha plate reader (PerkinElmer) to determine antibody specificity.

Preparation of HEK293T cell lysates overexpressing cGAS

One day before transfection, Human Embryonic Kidney (HEK)293T cells (ATCC) were plated at 5×10^5 cells/well in a 6-well plate. A *cGAS*-expression plasmid or a control plasmid was mixed with FuGENE HD (Promega, Madison, WI, USA) in OptiMEM (Thermo Fisher Scientific) according to manufacturer instructions. After a 10-min incubation, the mixture was added to the HEK293T plate. After a 2-day culture, cell lysates were prepared by suspending the cells of each well in 100 μL of cell lysis buffer [50 mM Tris-HCl (pH 7.5) containing 1% NP-40] to disrupt and solubilize the cell membrane, followed by centrifugation at 20,000*g* for 30 min. After centrifugation, the supernatant was collected to represent the cell lysate.

Analysis of multiple cell lines

At 1-day before transfection, FaDu human head and neck carcinoma cells, CT26 murine colon carcinoma cells, RAW264.7 murine leukemia macrophage cells, or 4T1 murine mammary carcinoma cells (ATCC) were plated at 2×10^4 cells/well in a 96-well plate, and dsDNA (90 bp; custom synthesized at Invitrogen, Carlsbad, CA, USA) mixed with Lipofectamine 3000 (Thermo Fisher Scientific) in OptiMEM according to manufacturer instructions were added to the plate. After a 1-day culture, the CT26, RAW264.7, and 4T1 cells in each well were suspended in 30 μL of cell lysis buffer [50 mM Tris-HCl (pH 7.5) containing 1% NP-40], followed by centrifugation at 20,000*g* for 30 min. After centrifugation, the supernatant was collected to represent the cell lysate and stored at −80°C until use. FaDu cells were incubated for 3 h with dsDNA. All other steps were as previously described.

Time-resolved fluorescence energy transfer (TR-FRET) analysis of cGAMP

To measure cGAMP concentration, I performed cGAMP-competitive TR-FRET. PBS containing 0.1% bovine serum albumin (Wako Pure Chemical Industries, Ltd.), and 0.005% Tween-20 was used as an assay buffer. To generate a standard curve, 5 μL of serially diluted cGAMP in assay buffer was mixed with 15 μL of cGAMP TR-FRET working solution containing 100 pM anti-cGAMP antibody #23, 1 nM Tb-labeled anti-mouse antibody (Life Technologies, Carlsbad, CA, USA), and 1 nM fluorescein isothiocyanate (FITC)-labeled cGAMP (BioLog) in assay buffer in 384-well plates. To measure cGAMP concentration, 5 μL of cell lysate or tissue lysate was mixed with 15 μL of cGAMP TR-FRET working solution. After a 1-h incubation, the TR-FRET intensities of the signals at 520 nm and 486 nm were measured using a Wallac ARVO X5 plate reader (PerkinElmer). cGAMP concentration was determined based on the obtained standard curve. Tissue lysates were prepared from the

hearts of wild type (WT) or *Trex1*-knockout (KO) mice. Heart tissues were minced and dissociated in cell lysis buffer [50 mM Tris-HCl (pH 7.5) containing 1% NP-40], followed by sonication treatment using MICROSON XL2000 (Misonix, Farmingdale, NY, US). The supernatant, representing the tissue lysate, was used in the TR-FRET assay after centrifugation at 20,000*g* for 30 min. The total protein concentration of the tissue lysates was measured by the Bicinchoninic acid (BCA) assay using a BCA protein assay kit (Thermo Fisher Scientific).

LC-MS detection of cGAMP

After a 1-day culture, FaDu cells were transfected with dsDNA in Lipofectamine 3000 (Thermo Fisher Scientific) and detached from the plate by trypsin/EDTA treatment. After washing with PBS, 1×10^6 cells were suspended in 500 µL of ice-cold methanol. The sample buffer was prepared by mixing 815 µL of distilled water, 100 µL of 1 mM EDTA, 35 µL of acetic acid, and 50 µL of octylamine, and 15 µL was added to 60 µL of the cell suspension, followed by centrifugation at 20,000g for 5 min and supernatant collection. The supernatant was analyzed by LC-MS. cGAMP concentration was determined based on the peak area generated using cGAMP-standard solution containing 0.5, 0.25, or 0.025 nmol of cGAMP in the sample buffer described above. For the measurement of tissue cGAMP, the hearts of *Trex1*-KO or WT mice (7-weeks old) were homogenized in saline into 20% (w/v). A total of 50 µL of tissue homogenate was added to 100 µL of methanol, followed by centrifugation at 20,000*g* for 5 min. The supernatant was applied to solid-phase extraction, and the resulting filtrate was analyzed by LC-MS. The cGAMP peak in the hearts of *Trex1*-KO mice was identified based on the peak of the cGAMP-standard solution, spiked at 0.1 ng/g in the heart homogenates from WT mice.

ICC detection of cGAMP in CT26 cells

CT26 cells were seeded into a 96-well plate at 1×10^4 cells/well and transfected with dsDNA in Lipofectamine 3000 (Thermo Fisher Scientific) after 1-day incubation. The medium was removed after 1-day culture, and PBS containing 4% paraformaldehyde (PFA) was added to fix cells at room temperature for 10 min. PFA fixation was repeated twice, and cells were washed with PBS three times. Fixed CT26 cells were permeabilized with PBS containing 2% normal donkey serum (Sigma-Aldrich, St. Louis, MO, USA) and 0.1% Tween-20 for 1 h, followed by addition of anti-cGAMP antibody #23 or mouse IgG2a isotype control antibody (R&D Systems, Minneapolis, MN, US) diluted to 1 µg/mL in PBS containing 2% normal donkey serum in the absence or presence of exogenously added cGAMP (BioLog) at a final concentration of 1 µM. After overnight incubation at 4°C, the cells were washed with Tris-

buffered saline (TBS) containing 0.1% Tween-20 (TBST). Hoechst 33342 (Molecular Probes, Eugene, OR, USA) and goat anti-mouse IgG (H+L) conjugated with Alexa Fluor 488 (Invitrogen) in TBST were added. The mixture was incubated 1 h at room temperature. After three washes with TBST, fluorescence was visualized using a fluorescence microscope (Olympus Corporation, Tokyo, Japan).

Animal welfare

Animals were cared for according to the Guide for the Care and Use of Laboratory Animals (National Research Council, 2011). Animals were socially housed at an Association for Assessment and Accreditation of Laboratory Animal Care-accredited facility at Takeda Pharmaceutical Co. Ltd. (Kanagawa, Japan). All animal-related research protocols were approved by the Takeda Institutional Animal Care and Use Committee.

Generation of Trex1-KO mice

A targeting vector for homologous recombination was constructed by insertion of a *loxP* site upstream of exon 2 of the *Trex1* gene and insertion of an FLP-recombinase-target sequence-flanked neomycin-resistance cassette with another *loxP* site downstream of exon 2 using bacterial artificial chromosome clone RP23-86F9 and a Red/ET recombination kit (GeneBridges, Heidelberg, Germany). The resulting vector was electroporated into C57BL/6J ES cells, as previously described (Yamamoto et al., 2013), and recombinant cells were selected using 200 μg/mL of geneticin G418 (Invitrogen). *Trex1*-KO ES cells were created by excision of *Trex1* exon 2 and the neomycin-resistance cassette following Cre-expression-vector electroporation. The resulting *Trex1*-KO cells were injected into tetraploid blastocysts from ICR mice (10-weeks old; CLEA Japan, Inc.), and chimeric offspring were identified according to the copy number of *Trex1* exon 2 and the neomycin-resistance cassette via real-time polymerase chain reaction (PCR). To generate *Trex1*-KO mice, chimeric male mice were used for *in vitro* fertilization of C57BL/6J female mice, and the genotype was confirmed by PCR using the following primer pairs: Trex1 wild-type (WT), 5'-CTCACCCCTGAAGGTAGTCAGCACTA-3' and 5'-CCAGCTCAGCTTTGCTCAGACCTGTGATCTCACTG-3'; and *Trex1*-KO 5'-CTCACCCCTGAAGGTAGTCAGCACTA-3' and 5'-AGACTCCGCACCCTCATTCTCAATA-3'.

Results and Discussion

Generation of the cGAMP antibody

To quantify cGAMP concentration in cells and detect cGAMP in tissues, I generated anti-cGAMP mAbs based on their broad usefulness in multiple assays, including ELISA, western blot, ICC, and immunohistochemistry (IHC). To this end, hybridoma techniques were used following immunization of CD2F1/Crlj mice with cGAMP-KLH. Since cGAMP is a small molecule relative to a protein or peptide antigen, I conjugated cGAMP to KLH as a carrier protein in order to account for the low antigenicity of cGAMP. To effectively obtain anti-cGAMP antibodies, an anti-mouse CD25 mAb was intraperitoneally injected into mice 2 days before the first immunization based on a previous finding that CD25-positive T cell depletion enhances the antibody response (Ndure and Flanagan, 2014).

The immunized mice were bled after the fifth and seventh immunizations to test antibody titers against cGAMP by cGAMP-Biotin ELISA. Antibody specificity was further evaluated relative to the cAMP-Biotin binding. After the fifth immunization, nine of ten mice showed increasing titers, specific to cGAMP (mice #1–7, 9, and 10; Fig. 1A). In the specificity assay, the plasma antibody of mouse #1 showed binding activity to cAMP-Biotin, although it was weak relative to its binding activity to cGAMP (Fig. 1A and B). After the seventh immunization, each immunized mouse showed a higher antibody titer to cGAMP relative to that observed after the fifth immunization (Fig. 1C). Although the specificity tests indicated binding to cAMP, specificity for cGAMP exceeded that for cAMP after the seventh immunization (Fig. 1D).

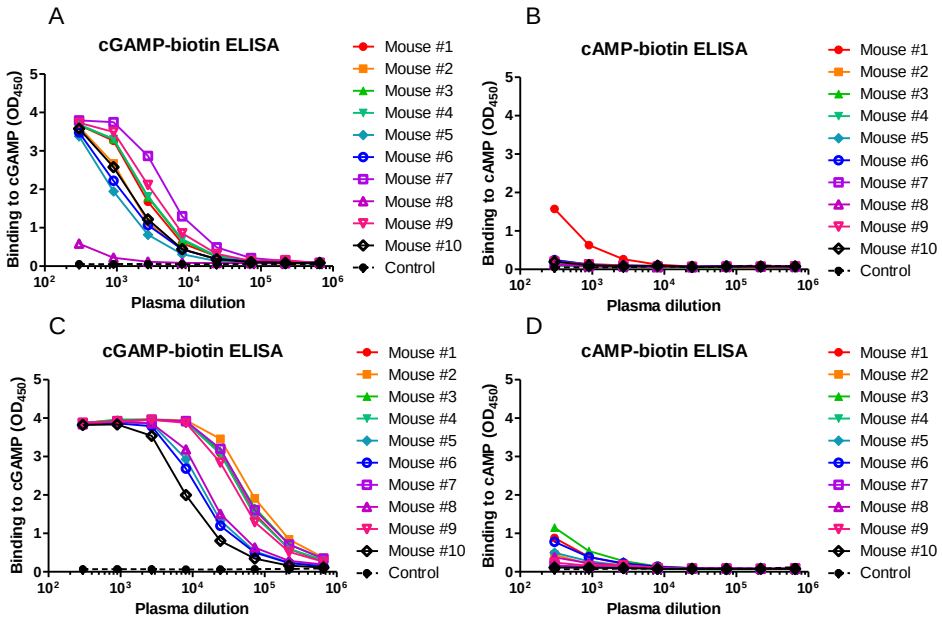

Fig. 1 Plasma titers of cGAMP-KLH-immunized mice. Plasma titer of each mouse at the (A, B) fifth and (C, D) seventh immunizations against (A, C) cGAMP-Biotin or (B, D) cAMP-Biotin. Control samples were prepared using plasma from non-immunized mice. Plasma titers were determined by ELISA. The vertical axis indicates binding to cGAMP or cAMP (OD_{450} values), and the horizontal axis indicates the plasma-dilution rate. Data points represent the OD_{450} values acquired in individual experiments and obtained in a single experiment.

I chose the four mice exhibiting the highest plasma titers and selective binding to cGAMP (mice #2, 4, 7, and 9; Fig. 1C and D), and screened the generated hybridomas using lymphocytes from popliteal lymph nodes in order to isolate cGAMP-specific antibodies. The assay identified 47 hybridoma clones producing antibodies specific to cGAMP from 2,000 wells of hybridomas. To determine the optimal anti-cGAMP mAb for highly-selective cGAMP quantification, I developed a competitive immunoassay rather than a sandwich assay in order to discriminate the specificity of the anti-cGAMP mAb, based on its small size. A competitive immunoassay uses competition between a labeled ligand (tracer) and an unlabeled ligand (analyte) for the binding site of an antibody, with only one antibody used to determine the analyte level and resulting in accurate evaluation of antibody specificity.

Additionally, I developed a high-throughput assay based on homogenous TR-FRET to enable the processing of a large number of samples in the absence of washing steps. In this homogenous competitive-immunoassay format, the 50% inhibitory concentration (IC_{50}) of an antibody to an analyte represents a key parameter for determining assay sensitivity. Because

the standard curve of a competitive-binding assay has a negative slope, an antibody with a lower IC_{50} value is capable of detecting lower concentrations of an analyte. Therefore, I determined the IC_{50} value of each antibody using an in-house cGAMP AlphaScreen assay and cGAMP-Biotin and unlabeled cGAMP. I found that 44 of the 47 antibodies showed IC_{50} values < 10 nM. I ultimately selected anti-cGAMP antibody #23 for further analysis because it had the lowest IC_{50} value (1.5 nM) (Fig. 2).

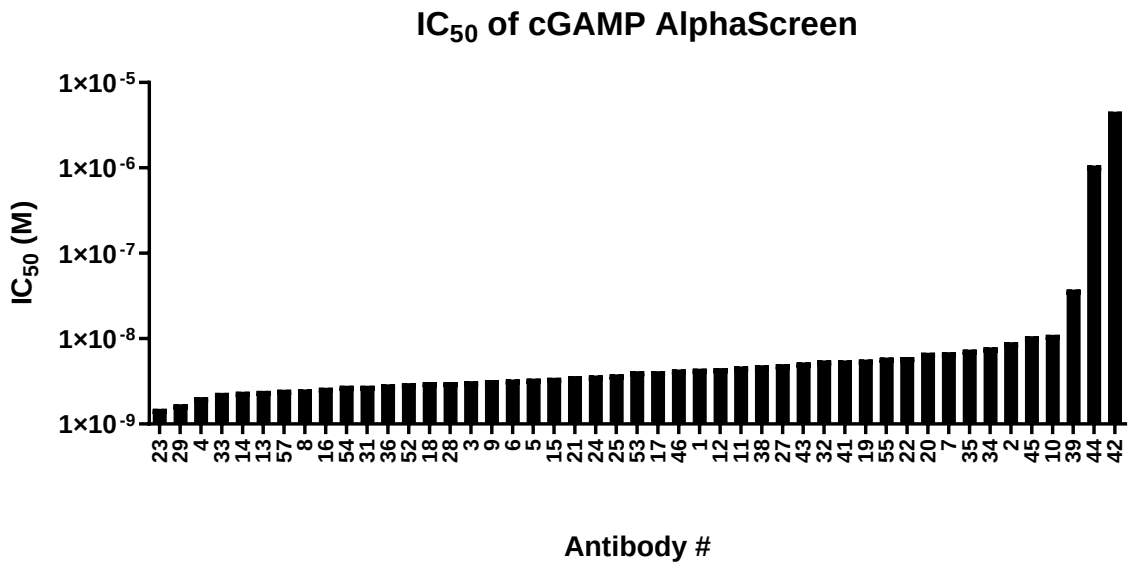

Fig. 2 Determination of the IC_{50} values of the purified mAbs. The IC_{50} values of 47 purified mAbs were determined by AlphaScreen. Anti-cGAMP antibody #23 showed the highest sensitivity. The vertical axis indicates the IC_{50} value of each mAb. Each bar represents the IC_{50} value acquired in individual experiments. The IC_{50} value was obtained in a single experiment.

Characterization of anti-cGAMP mAb #23

The affinity of anti-cGAMP antibody #23 to cGAMP was determined by SPR. The antibody was immobilized onto the sensor chip as a ligand, with cGAMP applied as an analyte. The K_D value of the anti-cGAMP antibody #23 to cGAMP was 14 nM, according to an analysis using a Langmuir fitting model (Fig. 3). The K_a of the antibody was determined at 1.20×10^5 (1/M/s) and the K_d at 1.71×10^{-3} (1/s). I tested the specificity and cross-reactivity of anti-cGAMP antibody #23 to other cyclic di-nucleotides and cyclic nucleotides (2'2'-cGAMP, 3'3'-cGAMP, c-di-GMP, c-di-AMP, cGMP, or cAMP). The results showed that anti-cGAMP antibody #23 bound cGAMP with high affinity and 2'2'-cGAMP and 3'3'-cGAMP with low affinity (IC_{50}: 2.9 nM, 2,400 nM, and 115 nM, respectively; Fig. 4A). Additionally, anti-

cGAMP antibody #23 did not bind c-di-GMP, c-di-AMP, cGMP, or cAMP. These results indicated that anti-cGAMP antibody #23 preferentially bound cGAMP, suggesting that it did not recognize the purine base or the ribose of cGAMP but did recognize the phosphodiester linkage between the guanosine and the adenosine (Fig. 4B–D).

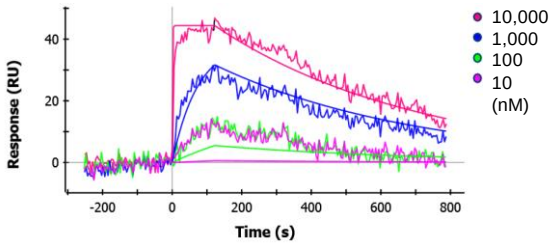

ka (1/Ms)	kd (1/s)	KD (M)
1.20×10^{5}	1.71×10^{-3}	1.42×10^{-8}

Fig. 3 Affinity of anti-cGAMP antibody #23 to cGAMP. SPR affinity analysis of anti-cGAMP antibody #23 to cGAMP. The vertical axis indicates the resonance unit (RU) of SPR response, and the horizontal line indicates the time after analyte injection. Kinetic parameters were analyzed using a 1:1 Langmuir fitting model. Association (K_a) and dissociation (K_d) rate constants were calculated and used to determine the K_D value (K_d/K_a). Each sensorgram was obtained in a single experiment. SPR affinity analysis was performed in more than two independent experiments.

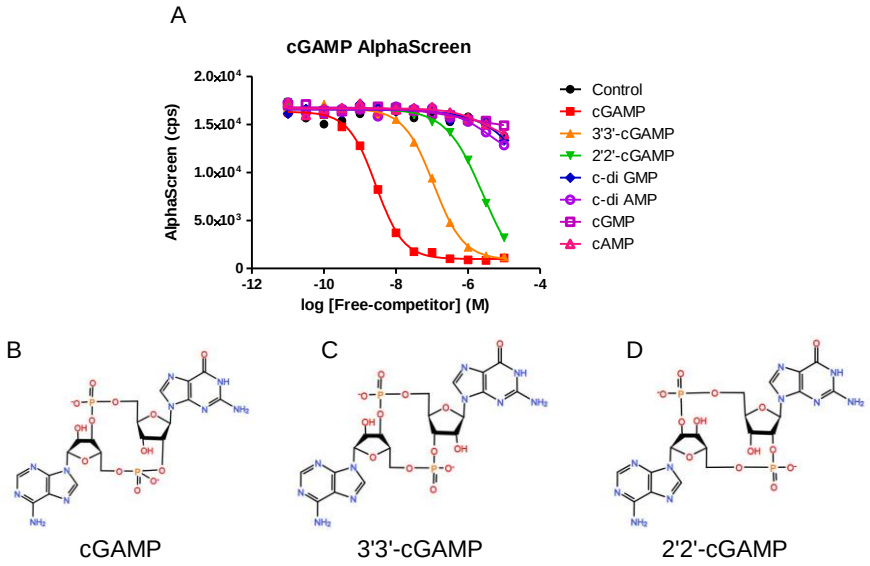

Fig. 4 Specificity of the anti-cGAMP antibody #23. (A) Specificity of the anti-cGAMP antibody #23 was determined by cGAMP AlphaScreen. cGAMP-Biotin (1 nM) and 100 pM of anti-cGAMP antibody #23 were mixed with various concentrations of competitor molecules (cGAMP, 2'2'-cGAMP, 3'3'-cGAMP, c-di-GMP, c-di-AMP, cGMP, or cAMP). The vertical axis indicates the AlphaScreen signal (counts/s; cps), and the horizontal axis indicates the concentration of free competitor. "Control" indicates a solution with no competitor. The data points indicate the mean of the Alphascreen signal acquired in duplicate. (B–D) Chemical structures: (B) cGAMP, c[G(2',5')pA(3',5')p] cyclic guanosine-(2'→5')-monophosphate-adenosine-(3' → 5')-monophosphate; (C) 3'3'-cGAMP, c[G(3',5')pA(3',5')p] cyclic guanosine monophosphate-adenosine monophosphate; (D) 2'2'-cGAMP, c[G(2',5')pA(2',5')p] cyclic guanosine-(2' → 5')-monophosphate-adenosine-(2' → 5')-monophosphate.

In cells and tissues, cGAS catalyzes the formation of cGAMP (2'3'-cGAMP) from GTP and ATP, but not 2'2'-cGAMP or 3'3'-cGAMP. Because only bacterial variable surface protein-1 synthesizes 2'2'-cGAMP and 3'3'-cGAMP (Davies et al., 2012), these variants do not exist in human cells and tissues. Therefore, the fact that anti-cGAMP antibody #23 binds to these compounds should not interfere with cGAMP measurements in human samples.

Development of a cGAMP-specific TR-FRET assay

Conventional ELISAs require multiple wash steps to remove excess reagent, resulting in

decreased throughput relative to homogenous assays. To establish a homogenous TR-FRET-based assay using anti-cGAMP antibody #23, I used Tb-labeled anti-mouse IgG and FITC-labeled cGAMP as a tracer. To optimize the concentration of FITC-labeled cGAMP, I investigated a competitive binding curve using serially diluted unlabeled cGAMP for TR-FRET analysis and a fixed concentration of anti-cGAMP antibody #23, as well as Tb-labeled anti-mouse IgG. Additionally, I increased the signal to background ratio in a tracer-concentration-dependent manner until saturation at 3 nM (Fig. 5A). Based on the competitive binding curve, I determined 1 nM as the optimal tracer concentration, with a quantifiable range determined according to the amount of analyte that decreased the TR-FRET signal (0.1–100 nM cGAMP; Fig. 5B). Furthermore, the cGAMP TR-FRET assay requires only 1 h, involves no wash steps, and is capable of measuring cGAMP concentration in 384-well formats at a sample volume of 5 µL/well.

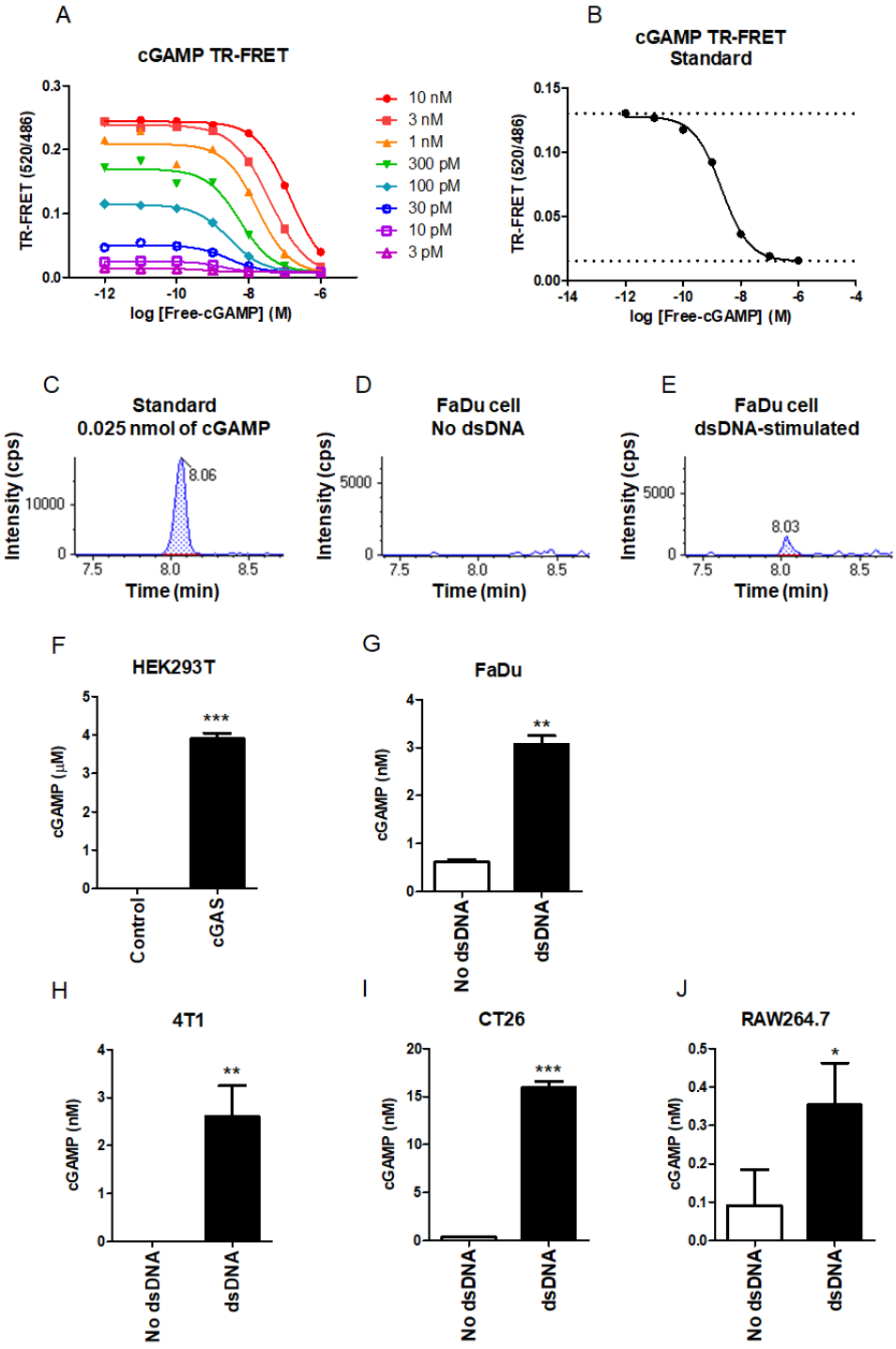

Fig. 5 TR-FRET analysis of cellular cGAMP concentration. (A) Optimization of the cGAMP TR-FRET assay. To determine the appropriate concentration range for the anti-cGAMP antibody #23, the antibody reacted to serially diluted cGAMP. The vertical axis indicates the normalized TR-FRET intensity (calculated as signal at 520 nm / signal at 486 nm), and the

horizontal axis indicates the concentration of free cGAMP. Data points indicate the mean of the TR-FRET signal acquired in duplicate. (B) Quantifiable range of the cGAMP TR-FRET assay. Using 1 nM of anti-cGAMP antibody #23, the detectable range of cGAMP TR-FRET was determined at 0.1 nM to 100 nM cGAMP. The vertical axis indicates the normalized TR-FRET intensity, and the horizontal axis indicates the concentration of free cGAMP. Data points represent the mean of the TR-FRET signal values acquired in duplicate experiments. The upper dotted line indicates the lower limit of detection, and the lower dotted line indicates the upper limit of detection. (C–E) cGAMP detection by LC-MS. (C) cGAMP peaks were detected using 0.025 nmol of a cGAMP standard, (D) non-dsDNA-treated FaDu cell lysate, or (E) dsDNA-treated FaDu cell lysate. The vertical axis indicates the intensity of the chromatogram (cps), and the horizontal line indicates the time after analyte injection (min). The numbers in the chromatograms indicate the times of the detected peaks. (F–J) cGAMP concentration in cell lysate measured by TR-FRET. (F) cGAMP concentrations were measured in lysates from HEK293T cells transfected with a cGAS-expressing vector or control vector and (G) from FaDu, (H) 4T1, (I) CT26, and (J) RAW264.7 cells in the absence or presence of dsDNA. The vertical axis indicates cGAMP concentration. Data points represent the mean + standard deviation of the cGAMP concentration acquired in triplicate. *$p \leq 0.05$; **$p \leq 0.01$; ***$p \leq 0.001$ as determined by Student's *t*-test (vs. control vector or non-dsDNA group). cGAMP concentrations below the detectable range of TR-FRET were regarded as zero. cGAMP measurement in each cell line was performed in more than two independent experiments.

LC-MS is capable of measuring endogenous cGAMP levels in cells and tissues (Ablasser et al., 2013; Sun et al., 2013; Wu et al., 2013; Gao et al., 2015; Gray et al., 2015), and a recent report showed MS screening of a small-scale library of cGAS inhibitors (Vincent et al., 2017). However, due to its throughput, MS-based approaches are inappropriate for screening the number of compounds necessary for drug-discovery purposes (Macarron et al., 2011; Karawajczyk et al., 2015). cGAMP TR-FRET assay in this study represents a high-throughput method that can be performed in a 384-well plate format, does not require any washing steps, and might be efficacious for identifying lead compounds from large compound libraries.

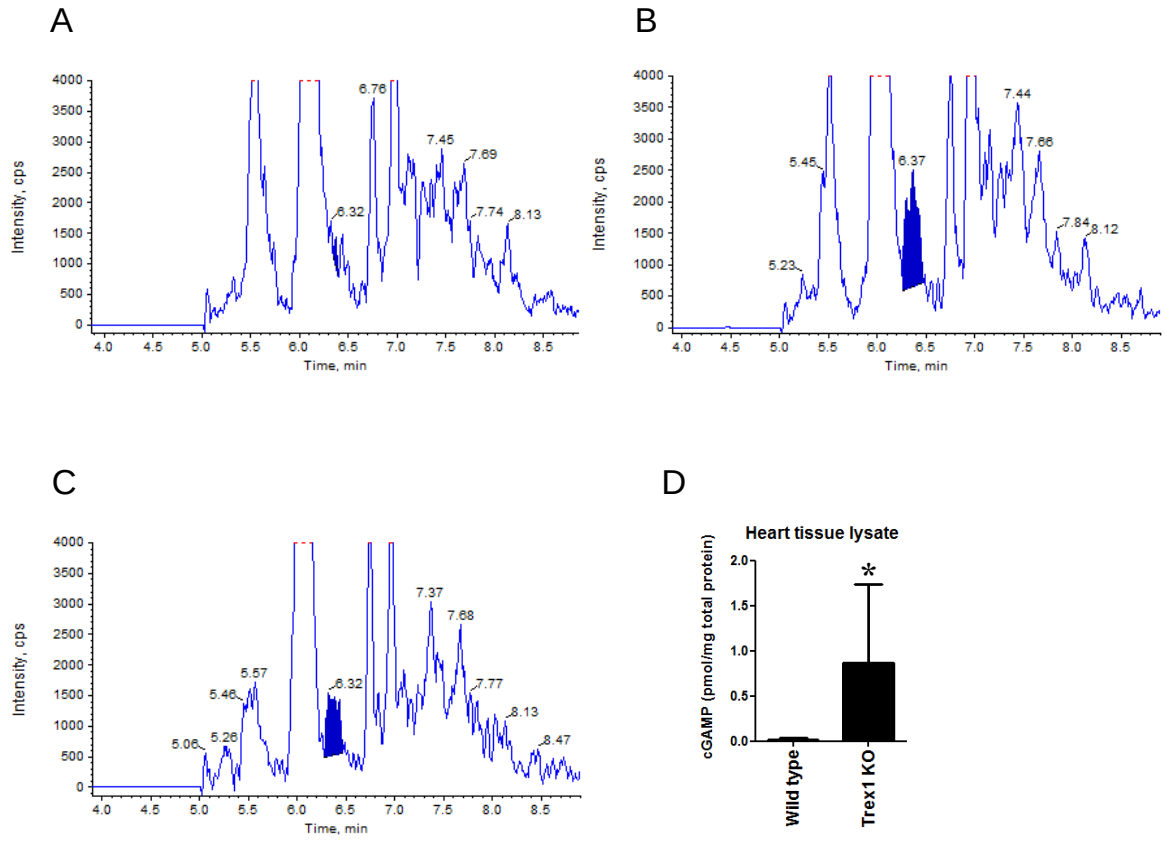

Fig. 6 TR-FRET analysis of cGAMP concentration in mouse tissue. (A–C) Tissue cGAMP detection by LC-MS. (A) Heart tissue lysate from WT mice. (B) cGAMP peaks were identified using 0.1 ng/g cGAMP standard spiked in the heart tissue homogenate from WT mice. (C) cGAMP peaks were detected in the heart tissue homogenate from *Trex1* KO mice. Solid blue peaks indicate cGAMP. The vertical axis indicates the intensity of the chromatogram (cps), and the horizontal axis indicates the time after analyte injection (min). The numbers in the chromatograms indicate the retention times of the detected peaks. (D) cGAMP concentrations were measured in lysates from the heart tissue of WT or *Trex1* KO mice in the TR-FRET assay. The vertical axis indicates cGAMP concentration. Data points represent the mean ± standard deviation of cGAMP concentration acquired in triplicate. *p ≤ 0.05 as determined by Student's *t*-test (compared to WT mice). cGAMP measurement was performed in two independent experiments.

TR-FRET detection of cGAMP

I used cGAS-overexpressing cells to ensure that cGAMP TR-FRET could detect cellular cGAMP as an indicator of cGAS activation. HEK293T cells were transiently transfected with

a cGAS-expression plasmid, and cell lysates were diluted 100-fold to allow cGAMP detection by TR-FRET within a quantifiable range. The results indicated that cGAMP concentration was highly upregulated by cGAS when compared to cGAMP concentrations in the control cells, which were below the detection limit of the assay (Fig. 5F). These results indicated that the cGAMP TR-FRET assay was capable of detecting increase cGAMP levels in response to cGAS activity.

To ensure that the cGAMP TR-FRET assay could detect cGAMP in cells expressing endogenous levels of cGAS, I first identified a cell line with an active cGAS pathway. I tested four cell lines, including FaDu human head and neck carcinoma cells, EOL-1 human eosinophilic leukemia cells, HL-60 human promyelocytic leukemia cells, and Caco-2 human colon adenocarcinoma cells, by determining the phosphorylation of IRF3, a downstream molecule of cGAS, as described previously (Kato et al., 2013).

Because FaDu was the only cell line that showed IRF3 phosphorylation in response to dsDNA among the cell lines tested, I confirmed cGAMP production in FaDu cells in response to cGAS stimulation (i.e., dsDNA) by LC-MS. Cells were treated with dsDNA in Lipofectamine 3000 for 3 h to activate cGAS, as previously described (Yang et al., 2015), and cGAMP concentration was calculated according to the peak generated by the standard. In the lysate of non-stimulated FaDu cells, cGAMP concentration was under the detection limit. In contrast, the cGAMP concertation after dsDNA treatment was ~1 nM in 1×10^6 cells/mL (Fig. 5C).

To determine the ability of the cGAMP TR-FRET assay to evaluate cGAMP concentration in FaDu cell lysates, cells were stimulated with dsDNA as described in the Materials and Methods. The subsequent cGAMP TR-FRET assay could detect cGAMP production in response to dsDNA treatment (Fig. 5G). Similar assays performed using 4T1, CT26, and RAW264.7 cells detected increased levels of dsDNA-stimulated cGAMP (Figs. 5H–J). These results demonstrated the efficacy of the cGAMP TR-FRET assay for measuring cGAMP concentration in cells endogenously expressing cGAS.

I then assessed if the TR-FRET assay could detect cGAMP in tissues by using *Trex1*-KO mouse tissue. Trex1 is the most abundant cytosolic exonuclease. Therefore, *Trex1*-KO mice have an active cGAS pathway (Gray et al., 2015). I generated *Trex1*-KO mice and endogenous cGAMP production in *Trex1*-KO mice was confirmed by LC-MS (Fig. 6A–C). The TR-FRET assay successfully detected endogenous cGAMP in the mouse tissue (Fig. 6D).

Previous studies described that using RI-based TLC or IEC to detect cGAMP produced from recombinant cGAS *in vitro* does not detect cellular cGAMP (Gao et al., 2013; Diner et al., 2013; Li et al., 2013a). Moreover, the use of an FP-based assay to identify cGAS inhibitors using recombinant cGAS protein failed to sensitively measure endogenous cGAMP

levels, despite the use of an anti-cGAMP mAb (Hall et al., 2017). Furthermore, using an RNA aptamer resulted in low specificity to cGAMP and sensitivity for endogenous cGAMP, with a reported a lower limit of detection of ~0.95 μM and a 1.6-fold higher signal-to-background ratio, even when using concentrated cell lysates (Bose et al., 2016).

These findings indicate that the cGAMP TR-FRET assay presented here is efficacious for highly sensitive detection (0.1–100 nM) and quantification of cGAMP in cells. The profiles of the current cGAMP-detection methods using cell lysates are summarized in Table 1. A commercially available cGAMP ELISA kit from Cayman Chemical (Ann Arbor, MI, USA) is suitable for detecting low concentrations of cGAMP based on its sensitivity. LC-MS shows the lowest sensitivity among the three methods and requires extended sample-processing steps involving protein precipitation. The method described in this study has the advantage of being able to detect cGAMP, 2'2'-cGAMP, or 3'3'-cGAMP separately.

The sensitivity of the TR-FRET method falls between that of the ELISA and LC-MS methods. However, its throughput is the highest due to its homogenous-assay system that does not require any washing steps and the 384-well format, which required as low as 5 μL of cell lysate. These characteristics supported my conclusion that the TR-FRET method is the best-fit for large-scale drug screening using cell lysates. Because each method has distinct advantages and disadvantages, it is important to consider the purpose of the cGAMP measurement to select the best approach.

Table 1. Comparison of cellular cGAMP quantification methods

	TR-FRET	ELISA[a]	LC-MS[b]
Sensitivity to cGAMP	0.1 nM	0.01 nM	0.64 nM
Cross-reactivity to 2′2′-cGAMP	0.11%	0.80%	Not available
Cross-reactivity to 3′3′-cGAMP	2.50%	<0.01%	Not available
Sample volume	5 μL	50 μL	300 μL
Sample processing	5 min (cell lysis)	5 min (cell lysis)	16 h (protein precipitation)
Throughput	1 h/384 samples	2.5 h to 16 h/96 samples	20 min/sample
Application	High-throughput drug screening	Highly sensitive cGAMP measurement	Multiplexed cGAMP measurement

Cross-reactivity was calculated by comparing the IC_{50} value of the tested cross-reactant (2'2'-cGAMP or 3'3'-cGAMP) with the IC_{50} value of the primary analyte (cGAMP).

[a] 2'3'-cGAMP ELISA kit (Cayman Chemical, Ann Arbor, MI, USA).

[b] Paijo et al., 2016.

cGAMP detection in cells by immunostaining

I performed immunostaining using anti-cGAMP antibody #23 to determine the ability of the antibody to detect cGAMP distribution and production in cells. A previous study reported that some antibodies of small molecules can be used to identify intracellular targets by ICC or IHC (Wiemelt et al., 1997). Visualization of second-messenger signaling molecules is widely used for the diagnostic detection of disease biomarkers and the monitoring of therapeutic drug efficacy. Because CT26 showed the highest cGAMP concentration in response to dsDNA, dsDNA-stimulated CT26 cells were stained with anti-cGAMP antibody #23 and a fluorescence-labeled secondary antibody for ICC detection following cell permeabilization. Although cGAMP fluorescence intensity was low in CT26 cells in the absence of dsDNA stimulation, the cytoplasmic fluorescence intensity of cGAMP increased after dsDNA stimulation (Fig. 7).

I further confirmed the specificity of the anti-cGAMP antibody #23 to cGAMP by staining CT26 cells with control IgG or anti-cGAMP antibody #23 in the presence of exogenously-added cGAMP to block the binding of anti-cGAMP antibody #23 to endogenous cGAMP. As shown in Fig. 7, the fluorescence intensity was not detectable when I added control IgG or exogenously-added cGAMP. I found a weak fluorescence when I added anti-cGAMP antibody #23 in the absence of dsDNA. I speculated that this corresponded to endogenous cGAMP detected by anti-cGAMP antibody #23 because the TR-FRET assay detected cGAMP in CT26 cells in the absence of dsDNA (Fig. 5I) and because the fluorescence was abolished by exogenously-added cGAMP (Fig. 7). These results indicated a successful ICC-mediated visualization of cellular cGAMP using the anti-cGAMP antibody #23.

In the present study, I found that the anti-cGAMP antibody #23 could detect the small molecule cGAMP. Previous studies showed a similar detection of cyclic AMP through ICC or IHC assays (Wiemelt et al., 1997; Hanson et al., 1998; Martínez et al., 2001). Wiemelt et al. (1997) proposed the following mechanism of protein conjugation in cAMP staining: cyclic cAMP was cross-linked to a protein by the addition of an acetyl- or succinyl-reactive group to the 2' hydroxyl on the ribose, this reactive group was covalently linked to protein carboxyl groups with ethylene dicarbamide. Then, cyclic AMP protein conjugates were stained by antibodies. I consider that cGAMP detection in this study is a consequence of a similar mechanism of protein conjugation.

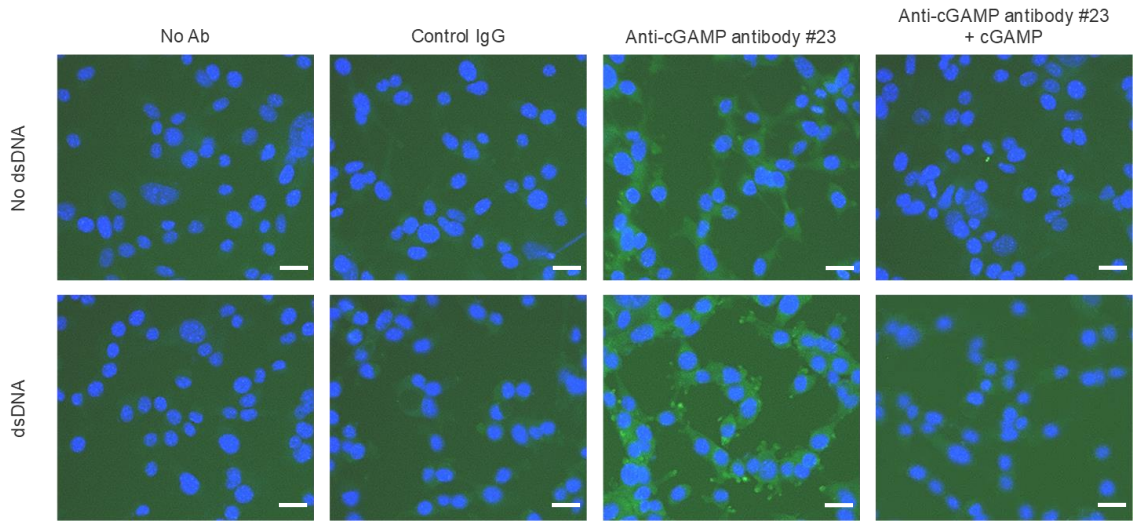

Fig. 7 ICC detection of cGAMP using anti-cGAMP antibody #23. Cellular cGAMP was detected by ICC using anti-cGAMP antibody #23. CT26 cells were incubated in the absence or presence of dsDNA. After fixation and permeabilization, CT26 cells were stained in the absence or presence of 1 μg/mL anti-cGAMP antibody #23 or control IgG with or without exogenously-added cGAMP, followed by incubation with anti-mouse IgG Alexa Fluor 488 (green). Nuclei were stained with Hoechst 33342 (blue). ICC detection of cGAMP was performed in three independent experiments. Scale bar: 10 μm.

Antibodies are widely used for clinical diagnostics and the monitoring of disease prognosis through ICC, IHC, ELISA, or flow cytometry. My TR-FRET and ICC results demonstrated the efficacy of the anti-cGAMP antibody #23 for the detection of endogenous cellular and tissue cGAMP. Moreover, this antibody promotes the performance of further cGAS-specific research to investigate the causality and potential as a therapeutic target of the cGAS-cGAMP-STING pathway in autoimmune diseases related to aberrant regulation of cytoplasmic DNA.

Conclusion

I have succeeded in demonstrating that the anti-cGAMP antibody generated in this study can be used for cGAMP TR-FRET assays to measure cGAMP concentration in cells and tissue, as well as for ICC assays to detect cGAMP distribution in cells. Anti-cGAMP antibody #23 represents a powerful tool that promotes the elucidation of cGAS involvement in autoimmunity and disease pathology at the molecular level. Furthermore, this antibody enables the distinction of cellular subpopulations using cGAMP as a biomarker in patients suffering from autoimmune diseases.

Chapter 2

Anti-sortilin1 antibody up-regulates progranulin via sortilin1 down-regulation

Abstract

Progranulin (PGRN) haploinsufficiency associated with loss-of-function mutations in the granulin gene causes frontotemporal dementia. This suggests that increasing PGRN levels could have promising therapeutic implications for patients carrying GRN mutations. In this study, I explored the therapeutic potential of sortilin1 (SORT1), a clearance receptor of PGRN, by generating and characterizing monoclonal antibodies against SORT1. Anti-SORT1 monoclonal antibodies were generated by immunizing *Sort1* knockout mice with SORT1 protein. The antibodies were classified into 7 epitope bins based on their competitive binding to the SORT1 protein and further defined by epitope bin-dependent characteristics, including SORT1-PGRN blocking, SORT1 down-regulation, and binding to human and mouse SORT1. I identified a positive correlation between PGRN up-regulation and SORT1 down-regulation. Furthermore, I also characterized K1-67 antibody via SORT1 down-regulation and binding to mouse SORT1 *in vivo* and confirmed that K1-67 significantly up-regulated PGRN levels in plasma and brain interstitial fluid of mice. These data indicate that SORT1 down-regulation is a key mechanism in increasing PGRN levels via anti-SORT1 antibodies and suggest that SORT1 is a potential target to correct PGRN reduction, such as that in patients with frontotemporal dementia caused by GRN mutation.

Introduction

Frontotemporal dementia (FTD) is a neurodegenerative disease characterized by the selective and progressive degeneration of the frontotemporal lobe. The disease is associated with progressive dementia, behavioral changes, and altered sociability and requires extensive medical care. Currently, the only available remedies for FTD involve symptomatic treatment that does not slow disease progression. Genome-wide association studies and mutation analysis of FTD patients have identified specific genes as risk factors for inherited FTD, including *GRN, C9orf72, MAPT, TMEM106B,* and *CST3* (Benussi et al., 2010; Pottier et al., 2016). *GRN* mutations are responsible for 5–20% of familial FTD cases and 1–12% of sporadic cases (Rademakers et al., 2012). Most *GRN* mutations result in a reduction in its protein product, progranulin (PGRN), via nonsense-mediated mRNA decay. This leads to PGRN haploinsufficiency (Ward and Miller, 2011). Patients with *GRN* mutations have reduced PGRN levels in their plasma, serum, or cerebrospinal fluid (CSF): only 30–50% of normal levels (Ghidoni et al., 2008; Mukherjee et al., 2008; Van Damme et al., 2008; Finch et al., 2009; Sleegers et al., 2009). These findings suggest that boosting PGRN levels could be a promising therapy for FTD treatment. A recent preclinical study has supported this notion by demonstrating that adeno-associated virus-driven expression of PGRN in the medial prefrontal cortex rescued social dominance deficits in a frontotemporal dementia model of *Grn* hetero-knockout (KO) mice (Arrant et al., 2017). Drug discovery research has also investigated PGRN-boosting therapies *in vitro* by targeting epigenetic factors and transcription factors (Capell et al., 2011; Cenik et al., 2011; Holler et al., 2016; Elia et al., 2020). However, these approaches have not been tested *in vivo*.

PGRN is a widely distributed pleiotropic protein that consists of seven and half cysteine-rich repeats (Mendsaikhan et al., 2019). In the brain, PGRN is secreted from microglia and acts as a neurotrophic factor, regulating a diverse range of cellular functions including cell proliferation, neuron survival, cell migration, neurite extension, lysosomal function, and anti-inflammatory responses (Toh et al., 2011; Kao et al., 2017). Sortilin 1 (SORT1), a type I transmembrane glycoprotein, is a clearance receptor of PGRN that acts by facilitating PGRN internalization (Hu et al., 2010). *SORT1* polymorphisms have been linked to PGRN levels in serum, as well as altered susceptibility to FTD and Alzheimer's disease (McMillan et al., 2014; Andersson et al., 2016; Philtjens et al., 2018; Tönjes et al., 2018), suggesting a key role of SORT1 in the regulation of PGRN levels. This notion is also supported by the observations that (1) *Sort1* KO raises *in vivo* PGRN levels by 2.5- to 5-fold and (2) *Sort1* ablation reverses the decrease in PGRN levels observed in *Grn* hetero-KO mice (Hu et al., 2010). In fact, the biotech company Alector is testing an anti-SORT1 antibody in

phase 3 clinical trials for the treatment of FTD, and is recruiting patients to evaluate the efficacy of the anti-SORT1 antibody (ClinicalTrials.gov, 2020).

In this study, I generated a variety of anti-SORT1 monoclonal antibodies (mAbs) to validate this hypothesis and establish their utility as potential therapeutics for FTD attributed to *GRN* mutations. Here, I describe the characteristics of these mAbs and discuss how they influence PGRN levels.

Materials and Methods

Animal welfare

All animal-related research protocols used in this study were approved by the Takeda Institutional Animal Care and Use Committee. Animals were handled according to the Guide for the Care and Use of Laboratory Animals (8th edition; National Research Council, 2011).

Generation of Sort1-knockout (KO) mice

Sort1 KO mice were generated as below. Briefly, an approximately 0.5 kbp region including exon3 of the Sort1 gene was deleted by using target site sequences of 5'-CTGCTTCAAGTGTAAGCGAT-3' and 5'-AAGAATCCATGAGATTCGCA-3' in C57BL/6J fertilized eggs by the CRISPR/Cas9 system. Resultant homozygous knockout mice were selected by testing the Sort1 exon3 sequence by qPCR. qPCR primer and probe sequences used were as follows: primers, 5'-TTGTCCCCTGCAGGTTATTCTC-3' and 5'-ACTGTCCAAAGCTCACAATTACCA-3'; MGB probe, 5'-TCCTGACCACTTTCCAAG-3'.

Generation of anti-SORT1 monoclonal antibodies

Sort1 KO mice (12-weeks old, male and female) were immunized as previously described (Kamala, 2007). Briefly, each mouse was injected subcutaneously in the hock with 5 μg of recombinant human SORT1 protein 5 times twice a week, followed by 5 injections of mouse SORT1 protein. TiterMax Gold (TiterMax) adjuvant was used in the primary immunization and was replaced with the mixture of ODN-1826 (InvivoGen) and aluminum hydroxide (Sigma-Aldrich) for the following boosts. One week after the tenth boost, the final boost was implemented by intraperitoneal injection of 10 μg of mouse SORT1 protein. Three days after the final boost, the lymphocytes from the mice were fused with P3X63Ag8U.1 mouse myeloma cells (ATCC) following standard procedures. Hybridoma selection and cloning were performed using ClonaCel-HY hybridoma kit (STEMCELL Technologies). Culture supernatants were collected from the wells of 96-well plates then screened by automated high-throughput FCM using 300-19 cell lines (purchased from Dr. Naomi Rosenberg's Lab, Tufts University) expressing human SORT1 or mouse SORT1. Selected hybridomas were cultured in Ham's F-12 nutrient medium (FUJIFILM Wako Pure Chemical) containing MEM non-essential amino acid solution (FUJIFILM Wako Pure Chemical), sodium pyruvate (FUJIFILM Wako Pure Chemical), L-alanyl-L-glutamine (FUJIFILM Wako Pure Chemical), penicillin and streptomycin (FUJIFILM Wako Pure Chemical), and 10% ultra-low IgG fetal bovine serum (Thermo Fisher Scientific) for antibody purification.

Preparation of recombinant proteins

DNA fragments encoding the extracellular domain of human or murine SORT1 fused with C-terminal 6 × His tag were synthesized and inserted into a pcDNA3.4 vector (Thermo Fisher Scientific). Chimeric proteins were prepared by reference to a previous report (Biilmann Rønn et al., 2016). DNA fragments encoding four chimeric proteins of human and puffer fish SORT1 were as below: nABcde, Met1-Arg77 (human)_Arg67-Ser98 (puffer fish)_Gly110-Pro343 (human)_Pro361-Ser773 (puffer fish); NabCDE, Met1-Arg109 (human)_Gly99-Val171 (puffer fish)_Ile202-Pro360 (puffer fish)_Ser344-Asn755 (human); NAbcDE, Met1-K254 (human)_Thr273-Gly538 (puffer fish)_Pro522-Asn755 (human); naBCdE, Met1-R77 (human)_Arg67-Val171 (puffer fish)_I202-Asp272 (puffer fish)_Ala255-Gly521 (human)_Pro539-Arg623 (puffer fish)_Asp606-Asn755 (human). These chimeric genes were fused to a 6 × His tag-encoding sequence and cloned into a pcDNA3.4 vector. A cDNA fragment encoding human furin M1-A595 C-terminally fused to Flag tag was synthesized and cloned into pcDNA3.4 vector. Recombinant proteins were produced with the Expi293F expression system (Thermo Fisher Scientific) according to manufacturer's protocol. Expi293F cells were transiently transfected with SORT1-encoding and furin-encoding plasmids and were incubated for 6 days. Culture supernatants were harvested and purified with Ni-NTA excel (GE Healthcare), followed by a SEC column (HiLoad 26/600 Superdex 200) from GE Healthcare.

Generation of stable cell lines

300-19 cell lines stably expressing human or mouse SORT1 were generated as previously described (Wang et al., 2018). In order to produce lentiviral particles, HEK293T cells (ATCC) were transiently transfected with pLenti6.2C-V5-DEST vector containing the full-length human mouse SORT1 gene together with Sigma Mission Lentiviral Packaging Mix (Sigma-Aldrich) by using Fugene 6 transfection reagent (Promega) according to the manufacturer's protocol. Culture medium containing virus was collected 48 h post transfection and precleaned by centrifugation at 2,000 g and filtration using a 0.45 μm filter unit (PALL Life Sciences). 300-19 cells were transduced with the viral supernatant and then selected with culture medium containing 1.5 or 9 μg/mL puromycin (Thermo Fisher Scientific) for human or mouse SORT1, respectively. Puromycin-resistant cells were maintained in the puromycin-containing selection medium for 10 days and subcloned by a limiting dilution. Outgrown cells were evaluated by FCM for the expression of human or mouse SORT1.

FCM screening

Hybridoma supernatant samples were screened according to an automated FCM method (Wang et al., 2018). 300-19 cells over-expressing human or mouse SORT1 were labeled with CellTrace Violet (Thermo Fisher Scientific) and Vybrant CFDA SE Cell Tracer (Thermo Fischer Scientific), respectively, following manufacturer's protocol. The cells were resuspended in cold phosphate-buffered saline (PBS) containing 2% fetal bovine serum (FCM buffer) and incubated with supernatant samples for 30 min at 4°C. After three rounds of washing using cold FCM buffer, 30 µL of Alexa Fluor 647 Anti-Mouse IgG (Jackson ImmunoResearch) was added. After 30 min of incubation at 4°C, the cells were washed twice with FCM buffer, and the binding of antibody was read on an iQue Screener PLUS (IntelliCyt).

Affinity measurement of anti-SORT1 antibody

An Octet Red96e system (Molecular Devices) based on biolayer interferometry was used to measure the kinetic parameters of the antibody. First, 10 µg/mL of antibody was captured using anti-mouse Fc (AMC) Octet biosensors (Molecular Devices) for 120 sec. Baseline was determined by an incubation of PBS containing 0.05% Tween-20 (PBST) alone for 60 sec. The mAb-capturing biosensors were reacted to recombinant human SORT1 protein at 200 nM to 3.13 nM (R&D Systems) for 120 sec followed by dissociation time of 180 sec in PBST. The kinetics of the antibody to SORT1 was analyzed with a sensorgram aligned at the beginning of the association step after a background subtraction. The sensorgrams were globally fit to a 1:1 Langmuir binding model.

Epitope mapping of anti-SORT1 antibody

The epitope mapping study was performed using the Octet Red96e system. Firstly, 10 µg/mL of mAbs were captured using AMC Octet biosensors for 120 sec followed by a baseline determination step of 60 sec in PBST. The biosensors were reacted to 30 µg/mL of human and chimeric SORT1 proteins for 120 sec followed by a dissociation time of 60 sec in PBST.

Epitope binning of anti-SORT1 antibody

The epitope binning of generated anti-SORT1 mAbs was performed by competitive sandwich enzyme-linked immunosorbent assay (ELISA). Briefly, the antibodies were immobilized on a 384-well plate (Corning). Separately, biotinylated SORT1 and anti-SORT1 antibody (competitor antibody) were pre-incubated at final concentrations of 100 nM and 1 µg/mL, respectively, and the complex was added to the antibody-coated 384 plate. Plate-bound

biotinylated SORT1 was detected using a horseradish peroxidase-conjugated StreptAvidin (Thermo Fisher Scientific) and SureBlue/TMB peroxidase substrate (SeraCare Life Sciences). The reaction was stopped by adding H_2SO_4, and the optical density at 450 nm (OD450) was measured using Wallac ARVO plate reader (PerkinElmer). The binding inhibition (%) was calculated using the following formula:

Binding inhibition (%) = (1–A/B) × 100,

where A represents the OD450 value of each well and B represents the OD450 value in a competitor antibody-free well. An epitope clustering was performed with the binding inhibition data by employing Ward's hierarchical clustering.

SORT1 binding ELISA

Binding activities of anti-SORT1 mAbs were tested using ELISA. Briefly, human or mouse SORT1 were immobilized on a 96-well plate and anti-SORT1 mAb was reacted to the plate-bound SORT1. SORT1-reactive mAb was detected using a horseradish peroxidase-conjugated anti-mouse IgG antibody (Jackson ImmunoResearch) and SureBlue/TMB peroxidase substrate. The reaction was stopped by adding H_2SO_4, and OD450 was measured using a SpectraMax 340PC384 plate reader (Molecular Devices).

Blocking ability of anti-SORT1 antibody against PGRN binding to SORT1

In brief, a human SORT1 expression vector and NeoFection reagent (astec) were mixed at a ratio of 1:1 in OptiMEM I (Thermo Fisher Scientific). After a 15-min incubation, the mixture was added to Expi293 cells at 1×10^6 cells/mL. Two days after the transfection, the cells were mixed with 0.3 μg/mL of biotinylated-PGRN (R&D Systems), 2 μg/mL of StreptAvidin-Alexa Fluor 647 (Thermo Fisher Scientific), and anti-SORT1 antibody in PBS containing 1% fetal bovine serum and 0.05% sodium azide. After a 3-h incubation, the cell surface fluorescence was detected by MirrorBall (TTP Labtech).

PGRN clearance assay with human U251 cells

U251 human glioblastoma cells (JCRB) were seeded at a density of 1×10^4 cells/well in a 96-well plate (Corning) in 100 μL of growth media MEM with Glutamax (Thermo Fisher Scientific) supplemented with 10% fetal bovine serum (Invitrogen) and 1% penicillin-streptomycin combination (FUJIFILM Wako Pure Chemical). The cells were incubated at 37°C and 5% CO_2 for 24 h and treated with the various concentrations of mAbs or PBS and incubated at 37°C and 5% CO_2 for 72 h. The isotype control antibody used was mouse IgG1 (Miltenyi Biotech). Cell supernatant was collected, and ELISA was performed using Human Progranulin DuoSet ELISA (R&D Systems) as per the manufacturer's instructions. OD450

was measured with the ARVO plate reader. Progranulin concentration was normalized against PBS-treated cells to identify relative changes in the progranulin levels.

Cortical neuron culture and PGRN clearance assay

Cortical neurons were isolated from E14 C57BL/6 wild-type (WT) mice. In brief, cortices from E14 mice were dissected and dissociated with Neuron Dissociation Solutions S (FUJIFILM Wako Pure Chemical) according to the manufacturer's instructions. Cells were seeded at a density of 7.5×10^4 cells/well on a Poly-D-Lysine-coated 96-well plate (Corning) and were grown in serum-free Neurobasal Medium (Invitrogen) with B-27 Supplement (Invitrogen), GlutaMAX (Gibco), and 100 U/mL of Penicillin-Streptomycin (Gibco). Half of the media was changed twice weekly. Neurons were used in PGRN clearance assays at 7 days *in vitro* (DIV). The cells were treated with anti-SORT1 mAb or control mouse IgG1 for 7 days. PGRN levels in collected culture media were determined with Mouse Progranulin DuoSet ELISA (R&D Systems) according to the manufacturer's instructions.

Detection of SORT1 down-regulation

Down-regulation of SORT1 was measured by immunocytochemistry-based image analysis. After the three-day treatment with anti-SORT1 antibodies (see the section of PGRN clearance assay), the U251 cells were washed with PBS and fixed with 4% paraformaldehyde. The fixed cells were permeabilized with 100 μg/mL of digitonin, incubated with 1 μg/mL of biotinylated anti-SORT1 polyclonal antibody (R&D Systems), and then stained with 2 μg/mL of streptavidin-conjugated Alexa 488 fluorescent dye. The cells were counterstained with 1 μg/mL of Hoechst 33342 (Thermo Fisher Scientific). All reactions were performed in the PBS containing 0.1% bovine serum albumin. Microscopic fluorescent images were obtained by In Cell Analyzer 6000 (GE Healthcare), followed by the image analysis using the In-Cell Developer program (GE Healthcare). The number of nuclei was used for normalization.

Plasma PGRN measurement

Three to four C57BL/6J mice (8 or 9-weeks old, male; CLEA Japan) were intravenously injected with anti-SORT1 antibody, clone K1-67, at 100 mg/kg. After 1 or 3 days, the mice were anesthetized with isoflurane to collect CSF and blood from the abdominal aorta by using heparin as an anticoagulant. The blood samples were centrifuged at 12,000 rpm for 10 minutes at 4°C for plasma isolation. Because of the small volumes obtained from each animal, CSF from 4 mice was pooled for PGRN measurement. PGRN levels were analyzed using a Mouse Progranulin Quantikine ELISA Kit (R&D Systems) according to the manufacturer's

protocol. Statistical analysis was performed (K1-67-treated versus PBS-treated groups) using the Aspin-Welch t-test.

Plasma K1-67 measurement

Plasma K1-67 levels were analyzed by immunocapture-liquid chromatography-mass spectrometry according to the procedure described in the literature (Hashii et al., 2018). Briefly, plasma K1-67 was immunocaptured by Dynabeads Protein G (Thermo Fisher Scientific) with a KingFisher Flex magnetic particle processor (Thermo Fisher Scientific), and then digested by trypsin (Promega). The digested samples were purified with Oasis MCX μElution plate (Waters) and then subjected to liquid chromatography-mass spectrometry. The peptide sequence of K1-67 (TAQATAYWGQGTLVTVSAAK) was specifically detected in the plasma and monitored by selected reaction monitoring analysis under the positive ion mode with a mass transition of m/z 1012.5 to 526.3 (precursor ion to product ion). Statistical analysis was performed (K1-67-treated versus PBS-treated groups) using the Aspin-Welch t-test.

Microdialysis

Mice were anesthetized using isoflurane. The skin over the skull was cut and separated from the skull surface. With bupivacaine topically applied to the skull, three small holes were made in the bone of the skull at the target site. Guide cannulas (CMA microdialysis) were placed into the holes. Sterile obturators were inserted into each guide cannula to prevent infections or the formation of obstructions and remained in place except during testing. Animals were allowed to recover for 7 days after surgery. Following the procedure, at least one post-operative dose of Rimydal 5 mg/kg and a second dose 24 hours later were administered. Twenty-four hours before the start of the microdialysis experiment, the animals were treated with PBS, K1-67 at 50 mg/kg or 100 mg/kg. On the day of the experiment, a 1,000 kDa cut-off probe (CMA Microdialysis) was inserted via the guide cannula into the hippocampus. The probe was connected to a microdialysis peristaltic pump (Microbiotech). The inlet tubing of the microdialysis probe was connected to a peristaltic pump perfusing the probe with artificial CSF. The peristaltic pump was also connected to the outlet tubing in order to prevent perfusion fluid loss from the probe, by pulling the fluid through the tubing. A perfusion buffer, 25% bovine albumin fraction V (Sigma-Aldrich), was diluted to 0.2 % with artificial CSF (147 mM NaCl, 2.7 mM KCl, 1.2 mM $CaCl_2$, 0.85 mM $MgCl_2$) on the day of use. The pump was set to a constant flow of 1 μL/min. A 2-h sampling regimen was used throughout the experiment providing 12 samples over a 24 h collection period. Statistical analysis was

performed (K1-67-treated versus PBS-treated groups) using the two-way RM ANOVA analysis with Sidak's multiple comparisons.

Results

Generation of anti-SORT1 mAbs

To assess whether reducing SORT1 function can up-regulate extracellular PGRN levels, I generated and characterized anti-SORT1 mAbs, that were cross-reactive to human and mouse SORT1. To do this, I first immunized WT mice with human SORT1 recombinant protein but unfortunately this approach produced anti-SORT1 antibodies that bound to human but not to mouse SORT1, perhaps because of immunotolerance to self-antigen. In an attempt to overcome this failure, I next decided to use Sort1 KO mice, naïve to mouse SORT1, and immunized them with human SORT1 protein (first to fifth immunization) and mouse SORT1 protein (sixth to tenth immunization) sequentially. To effectively obtain anti-SORT1 mAbs, an anti-mouse CD25 mAb was intraperitoneally injected into 4 Sort1 KO mice 2 days before the first immunization. This tactic was utilized based on a previous finding that CD25-positive T cell depletion enhances antibody response (Ndure and Flanagan, 2014). The immunized mice were bled after the fifth and ninth immunizations to establish antibody titers against SORT1 by flow cytometry (FCM) using SORT1 expressing cells. I sacrificed the mice and screened hybridomas derived from lymphocytes from popliteal lymph nodes to identify anti-SORT antibody expressors. The assay identified 29 hybridoma clones producing antibodies which cross-reacted to human and mouse SORT1 from 2,300 wells of hybridomas. The 29 anti-SORT1 mAbs were then purified from hybridoma supernatants for further characterization.

Characterization of anti-SORT1 mAbs

To characterize the anti-SORT1 mAbs, I performed multiple *in vitro* assays including binding ELISA, epitope binning, PGRN up-regulation assay using human and mouse cells, SORT1 down-regulation assay, and PGRN-SORT1 blocking assay. First, I confirmed the binding of mAbs to human and mouse SORT1 by ELISA and found that each anti-SORT1 mAb showed different binding characteristics toward human and mouse SORT1. These results indicate that those human and mouse cross-reactive anti-SORT1 mAbs have a wide range of cross-reactivity (Table 2).

I then classified anti-SORT1 mAbs by epitope binning based on a competitive sandwich ELISA method. Epitope binning is widely used for clustering mAbs by the competitive binding pattern among mAbs. To perform epitope binning, anti-SORT1 mAb was immobilized in an ELISA plate, and then a complex of a different anti-SORT1 mAb (competitor mAb) and SORT1 protein was added to the plate. Wherever epitopes of the immobilized mAb and competitor mAb did not overlap, SORT1 protein can be captured by

both the mAbs separately. However, when epitopes of immobilized mAb and competitor mAb overlap, immobilized mAb and competitor mAb competitively bind to SORT1, and the competitive binding can be detected as a reduced signal of competitor mAb (biotinylated). The competitive sandwich ELISA result was obtained as the 29 × 29 matrix of binding inhibition (%). After Ward's hierarchical clustering, the 29 mAbs fell into 7 bins (Fig. 8A).
I then determined the binding region of mAbs of each epitope bin in the following epitope mapping study. It has previously been reported that the extracellular domain of the SORT1 protein consists of three domains; a ten-bladed β-propeller and two 10CC domains (10CC-a and 10CC-b) (Quistgaard et al., 2014). Based on this information, I generated chimeric SORT1 proteins of human and a xenogenic species by domain-swapping. I renamed the domains for the purpose of convenience in this study. Since mature SORT1 is released by furin cleavage from its proform at amino acid residue 77 (Petersen et al., 1997), I used this information to design chimeric proteins : N-terminal region (Arg77-Arg109), A region (1-3 β-propeller blade), B region (4-5 β-propeller blade), C region (6-8 β-propeller blade), D region (9-10 β-propeller blade), and E region (10CC-a and 10CC-b).

For this purpose, I chose *Takifugu rubripes* (Japanese pufferfish) SORT1 protein (UniProt accession H2RV63), which shares 56.2% amino acid identity with human SORT1 (UniProt accession Q99523). I generated 4 chimeric proteins; nABcde (human SORT1 A, B and puffer fish SORT1 N-terminal, C, D, E regions), NabCDE (human SORT1 N-terminal, C, D, E and puffer fish SORT1 A, B regions), NAbcDE (human SORT1 N-terminal, A, D, E and puffer fish SORT1 B, C regions) and naBCdE (human SORT1 B, C, E and puffer fish SORT1 N-terminal, A, D regions) (Fig. 8B). The binding of anti-SORT1 mAbs to the chimeric SORT1 proteins was detected by biolayer interferometry (BLI). Anti-SORT1 mAb was captured by AMC biosensor, and then chimeric SORT1 proteins were applied as an analyte. I applied 6 anti-SORT1 mAbs (K1-19, K1-12, K1-15, K1-40, K1-67, and K1-05) as representatives of epitope bins I, II, III, V, VI and VII, respectively, in this epitope mapping study. Due to the low binding of epitope bin IV mAbs to human SORT1 protein, I did not include epitope bin IV mAb in this epitope mapping study. Each anti-SORT1 mAb demonstrated a distinctive binding pattern. Epitope bin I mAb, K1-19 bound to nABcde and NAbcDE, as well as to human SORT1 (Fig. 8C). Meanwhile, K1-19 failed to bind to NabCDE and naBCdE (Fig. 8C). These results indicate that K1-19 binds to the A region, which is shared among chimeric proteins. Similarly, other anti-SORT1 mAbs were analyzed and their epitopes were mapped by their chimeric protein binding patterns. The epitope of K1-12, K1-15, K1-40, K1-67, or K1-05 were identified as C, D, B, E, or D region, respectively (Fig. 8C to 8I).

Recent discoveries have demonstrated that SORT1 is a clearance receptor for PGRN,

promoting PGRN endocytosis and thereby determining plasma PGRN levels (Hu et al., 2010). This led me to investigate whether anti-SORT1 mAbs increased the PGRN concentration in the extracellular environment by blocking SORT1 function. I treated U251 human glioblastoma cells, which have the inherent capacity to release PGRN, with the anti-SORT1 antibody (Li et al., 2017). In the U251 PGRN assay, 19 out of 29 mAbs tested showed more than a 1.5-fold increase of extracellular PGRN compared to the control group (Table 2). However, a few among the 29 mAbs had no impact on extracellular PGRN levels. I then assessed whether mAbs were able to demonstrate a similar effect in mouse by using primary cortical neurons. Among the 29 mAbs, 18 mAbs raised extracellular mouse PGRN by more than 1.5 times compared to that in the control group. Intriguingly, 14 out of the 18 mAbs were among the 19 mAbs increasing human PGRN levels in the U251 assay. The exceptions were clones K1-02, K1-05, K1-06, and K1-07 demonstrating a mouse-specific PGRN increase, likely due to their relatively weak human versus mouse SORT1 binding ability as per the binding ELISA data (Table 2). I then assessed if there was a correlation between SORT1-binding and PGRN up-regulation between species. ELISA binding activity of anti-SORT1 mAb was found to be linked to the extent of PGRN up-regulation (Pearson correlation coefficient: human species, $r = 0.63$, $p = 2.8 \times 10^{-4}$; mouse species, $r = 0.56$, $p = 1.4 \times 10^{-3}$). These results suggested that the ability of an anti-SORT1 mAb to up-regulate PGRN was dependent on its binding affinity to SORT1. ELISA binding activities of anti-SORT1 mAbs to human and mouse SORT1 also showed a moderate correlation ($r = 0.43$, $p = 0.02$). However, the correlation between human and mouse PGRN up-regulation was not significant ($r = 0.27$, $p = 0.16$).

A

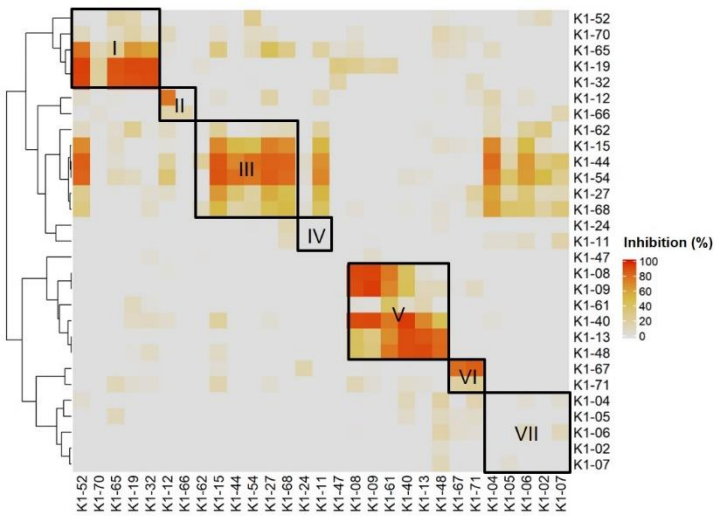

B

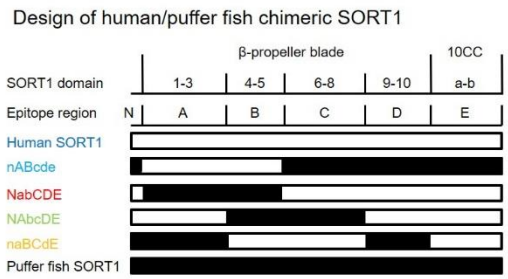

C D E

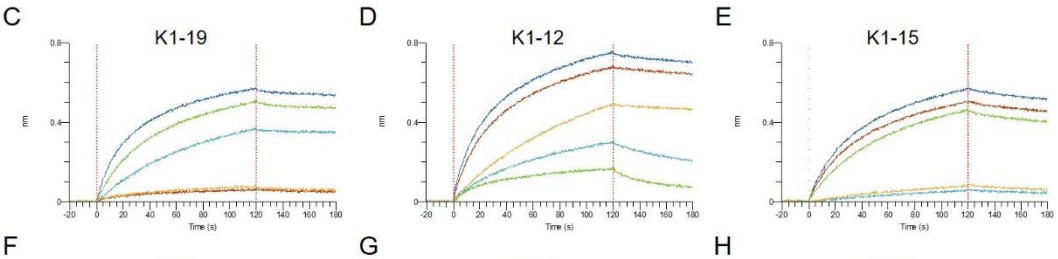

F G H

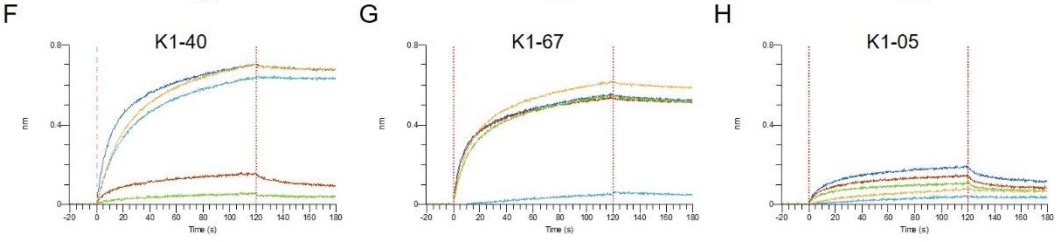

I

Epitope bin	Clone	Epitope region	SORT1 domain
I	K1-19	A	1-3
II	K1-12	C	6-8
III	K1-15	D	9-10
V	K1-40	B	4-5
VI	K1-67	E	10CC
VII	K1-05	D	9-10

Fig. 8 Binding profiles of anti-SORT1 mAbs. (A) Epitope binning of anti-SORT1 mAbs. The competitive binding was measured in a sandwich ELISA with 29 anti-SORT1 mAbs. Each column and row in the matrix represent an unlabeled and biotinylated anti-SORT1 mAb. The competitive binding of the 29 anti-SORT1 mAbs is shown as a heat map analyzed by Ward's hierarchical clustering. The color scale from 0 to 100 shows the competitive binding of the 2 mAbs. (B) Design of chimeric proteins; nABcde (human SORT1 A, B and puffer fish SORT1 N-terminal C, D, E regions), NabCDE (human SORT1 N-terminal, C, D, E and puffer fish SORT1 A, B regions), NAbcDE (human SORT1 N-terminal, A, D, E and puffer fish SORT1 B, C regions) and naBCdE (human SORT1 B, C, E and puffer fish SORT1 N-terminal, A, D regions). The white bar indicates the SORT1 domain derived from human and the black bar indicates the SORT1 domain derived from puffer fish. (C to H) Epitope mapping of anti-SORT1 mAbs. Epitope mapping was analyzed by the binding pattern of anti-SORT1 mAb to human/puffer fish chimeric SORT1 proteins in BLI. The BLI analysis was performed with anti-SORT1 mAb K1-19 (C), K1-12 (D), K1-15 (E), K1-40 (F), K1-67 (G), and K1-05 (H) as ligands and chimeric SORT1 protein as an analyte. The vertical axis indicates the BLI signal response (nm). The horizontal axis indicates the time after analyte loading. The sensorgram indicates as follows, dark blue: Human SORT1, light blue: nABcde, red: NabCDE, green: NAbcDE and yellow: naBCdE. (I) Epitope mapping results of anti-SORT1 mAbs tested are shown.

To investigate the molecular mechanisms by which anti-SORT1 mAbs increased PGRN levels, I conducted two assays based on the following assumptions: anti-SORT1 mAb would inhibit PGRN binding to SORT1 and/or would decrease membrane-bound SORT1 levels by down-regulating SORT1 protein. First, I performed SORT1-PGRN interaction analysis in which biotinylated PGRN remained on cells transiently over-expressing human SORT1 was detected in the presence of anti-SORT1 mAb. Fifteen out of 29 mAbs were able to block the SORT1-PGRN interaction by more than 50% at 15 μg/mL. The inhibitory activity of mAb against the SORT1-PGRN interaction showed no significant correlation with PGRN up-regulation (human species, $r = -0.23$, $p = 0.23$; mouse species, $r = 0.28$, $p = 0.14$). I then tested how anti-SORT1 mAb would affect membrane-bound SORT1 levels. In my study, 29 mAbs down-regulated SORT1 protein levels to different extents (Table 2). This effect was found to have a moderate correlation between human and mouse ($r = 0.47$, $p = 0.01$). Intriguingly, the SORT1 down-regulation was strongly correlated with PGRN up-regulation in human species ($r = 0.9$, $p = 2.7 \times 10^{-11}$) and moderately in mouse species ($r = 0.63$, $p = 1.7 \times 10^{-4}$). These findings indicate that SORT1 down-regulation triggered by the anti-SORT1 mAbs contributed to the up-regulation of PGRN.

These characterization assays define epitope bin-dependent activities of the anti-SORT1 antibodies. Some antibodies, such as K1-19 and K1-32, up-regulated PGRN levels only in human cells. Both antibodies belonged to epitope bin I and only showed strong binding to the human SORT1 molecule, suggesting that the epitope recognized by bin I mAbs is a human-specific sequence in SORT1. K1-12 in epitope bin II showed a moderate PGRN up-regulation in both human and mouse cells. On the other hand, epitope bin VII mAbs, such as K1-05, showed moderate PGRN up-regulation in mouse neurons but almost no activity in human cells. K1-67 from epitope bin VI showed a strong PGRN up-regulation in both human and mouse cells with high SORT1 down-regulation. The anti-SORT1 mAbs derived from bin III and bin VII blocked the SORT1-PGRN interaction. Both bin III and bin VII mAbs interacted with the D region of the SORT1 molecule. The bin III mAbs did not show strong SORT1 down-regulation, while bin VII mAbs did. These results clearly demonstrate the epitope bin defining characteristics of the antibodies discovered in this study.

Through this profiling, I found that SORT1 down-regulation was strongly correlated with PGRN up-regulation. The epitope bin VI mAb, K1-67 was selected for further evaluation due to its human and mouse cross-reactivity, high SORT1 down-regulation, potent PGRN up-regulation, and no PGRN-SORT1 interaction blocking activity.

Table 2. Summary of anti-SORT1 mAb characteristics.

Clone	Epitope bin[a]	hSORT1-His ELISA[b]	hPGRN-hSORT1 binding[c]	Human U251 cell		mSORT1-His ELISA[f]	Mouse primary neuron		Function[i]
				SORT1 down-regulation[d]	PGRN up-regulation[e]		SORT1 down-regulation[g]	PGRN up-regulation[h]	
		(OD @450nm)	(% inhibition)	(% control)	(fold-change)	(OD @450nm)	(% control)	(fold-change)	(PGRN competition or SORT1 down-regulation)
K1-19	I	1.44	13.2	95.4***	2.40***	0.78	4.2	1.13*	SORT1 down-regulation
K1-32	I	1.48	22.7	95.7***	2.20***	0.83	15.7	1.14*	SORT1 down-regulation
K1-52	I	0.19	80.5	44.1***	1.10*	0.94	17.3	1.17*	
K1-65	I	0.95	14.2	85.9***	1.70**	0.53	19.6	1.19	
K1-70	I	0.31	17.7	4.3	1.00	0.46	11.7	1.09*	
K1-12	II	0.78	58.1	87.1***	1.80***	0.78	53.5**	2.32***	
K1-66	II	0.14	34.6	31.9***	1.00	0.19	16.6	1.40**	
K1-15	III	0.70	90.7	71.1***	2.00**	1.36	17.0*	2.49***	PGRN competition
K1-27	III	0.49	76.9	76.2***	1.90*	1.43	28.8*	1.47**	
K1-44	III	0.41	89.8	75.7***	1.96***	1.04	36.4**	1.83***	
K1-54	III	0.54	99.5	75.1***	1.90**	1.33	33.6*	1.74**	PGRN competition
K1-62	III	0.22	96.3	13.7	1.00	0.15	5.4	1.14*	PGRN competition
K1-68	III	0.38	86.1	80.1***	2.00**	1.23	40.5*	1.65**	
K1-11	IV	0.25	99.2	62.6***	1.90**	1.17	35.7*	1.83*	PGRN competition
K1-24	IV	0.16	27.1	63.8**	1.40**	0.23	46.7**	1.39**	
K1-08	V	1.83	41.6	88.2***	2.00***	1.57	66.4**	1.80***	
K1-09	V	1.97	47.2	84.7***	1.60**	1.76	67.2**	1.78**	
K1-13	V	1.91	31.9	95.0***	1.90**	1.86	53.1**	1.55**	SORT1 down-regulation
K1-40	V	2.01	14.5	94.1***	2.30***	1.90	65.5**	2.11***	SORT1 down-regulation
K1-47	V	0.32	22.1	7.4	0.90	0.43	9.8	1.06	
K1-48	V	1.62	-3.5	95.4***	1.80**	1.83	62.2**	2.29**	SORT1 down-regulation
K1-61	V	1.42	33.6	85.1***	1.60***	1.17	53.9**	1.70**	
K1-67	VI	1.00	63.0	95.2***	1.90**	0.28	67.7***	2.07***	SORT1 down-regulation
K1-71	VI	0.43	46.8	88.1***	1.90**	0.14	37.9***	1.28*	
K1-02	VII	0.07	86.6	31.7**	1.10	1.37	43.1**	2.01**	
K1-04	VII	0.37	95.0	58.9***	1.60**	1.57	31.4*	1.78**	PGRN competition
K1-05	VII	0.13	102.0	16.2**	1.00	1.37	36.4**	1.83***	PGRN competition
K1-06	VII	0.13	101.4	31.1**	1.10	1.62	40.2*	1.89**	PGRN competition
K1-07	VII	0.17	100.0	12.1**	1.10	1.44	42.4**	1.70**	PGRN competition

[a] Epitope bin was determined by competitive binding profiles of anti-SORT1 mAbs in sandwich ELISA.

[b, f] Binding activity of anti-SORT1 mAb is shown as absorbance at 450 nm determined using ELISA.

[c] PGRN-SORT1 interaction block by anti-SORT1 mAb was calculated as a % inhibition at 15 μg/mL (vs PBS-treated control group).
[e, h] PGRN up-regulation by anti-SORT1 mAb was calculated as a fold-change (vs PBS-treated control). *; $p < 0.05$, **; $p < 0.01$, ***; $p < 0.001$ vs PBS-treated group by Student's t-test.
[d, g] SORT1 down-regulation is represented as SORT1 levels down-regulated from cell surface in response to anti-SORT1 mAb. *; $p < 0.05$, **; $p < 0.01$, ***; $p < 0.001$ vs PBS-treated group by Student's t-test.
[i] The inhibition of the interaction between PGRN and SORT1 in more than 90% was classified as PGRN competition. The down-regulation of SORT1 in more than 90% was classified as SORT1 down-regulation.

Characterization of anti-SORT1 mAb K1-67

In the first set of experiments I tested the concentration-dependency of PGRN up-regulation by K1-67 using U251 cells and mouse primary neurons. K1-67 up-regulated PGRN levels in both U251 cells and mouse primary neurons in a concentration-dependent manner with EC50 values of 0.14 and 2.14 μg/mL, respectively (Fig. 9A and 9B). I also determined the affinity of K1-67 to SORT1. The K_D values of K1-67 to human and mouse SORT1 were 1.87×10^{-9} M and 7.63×10^{-8} M, respectively, according to an analysis using a Langmuir fitting model (Fig. 9C and 9D). The K_a of the antibody was 2.02×10^5 (1/M/s) and the K_d was 3.77×10^{-4} (1/s) towards human SORT1. Meanwhile, the K_a of K1-67 was 3.13×10^4 (1/M/s) and the K_d was 2.39×10^{-3} (1/s) towards mouse SORT1.

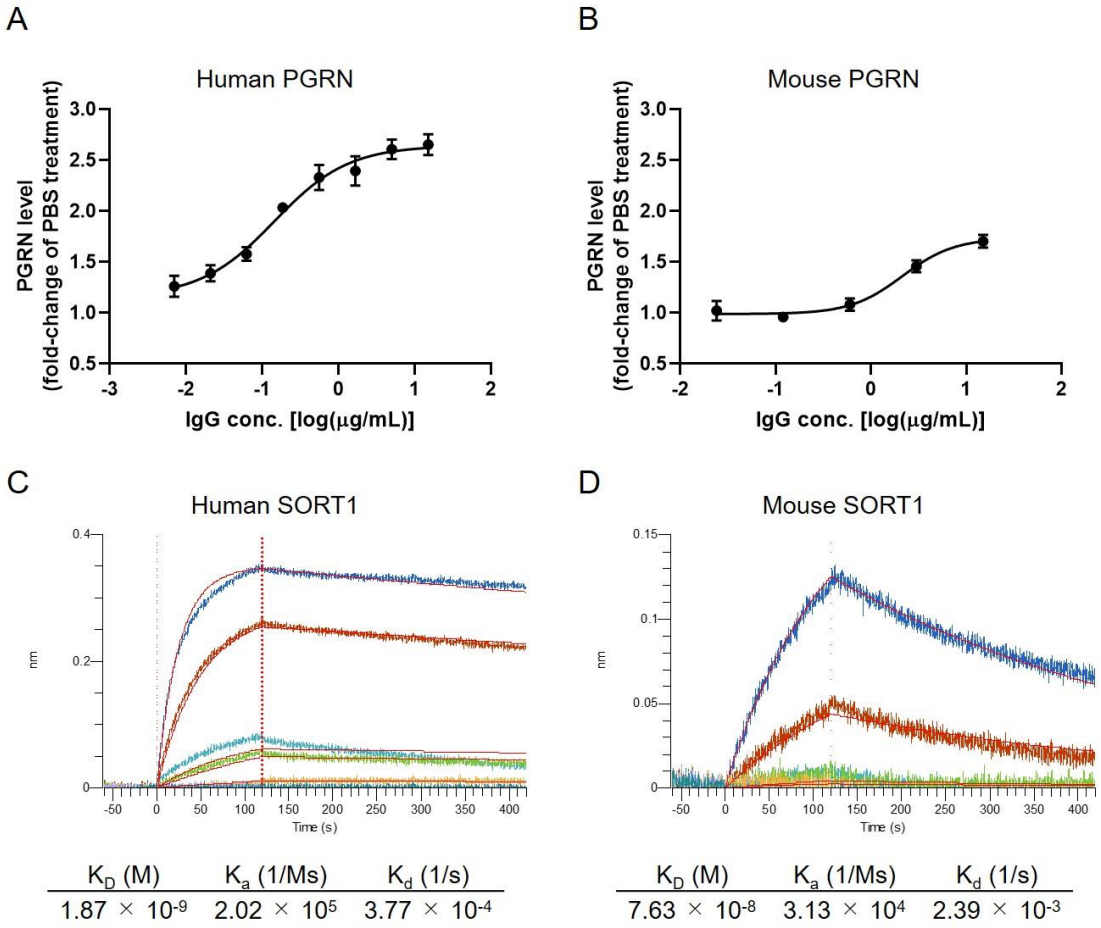

K_D (M)	K_a (1/Ms)	K_d (1/s)
1.87×10^{-9}	2.02×10^{5}	3.77×10^{-4}

K_D (M)	K_a (1/Ms)	K_d (1/s)
7.63×10^{-8}	3.13×10^{4}	2.39×10^{-3}

Fig. 9 Detailed characterization of anti-SORT1 mAb K1-67. (A) PGRN up-regulation in response to K1-67 in U251 human glioblastoma cells. Cells were treated with various concentrations of K1-67 for 72 hours. Human PGRN in U251 culture supernatant was determined by ELISA and is shown as a fold-change relative to PBS-treated cells. Data are mean ± SEM from 3 independent experiments. (B) PGRN up-regulation in response to K1-67 in mouse primary neurons. Cells were treated with various concentrations of K1-67 for 7 days. Mouse PGRN in mouse primary neuron culture supernatant was determined by ELISA and is shown as a fold-change relative to PBS-treated cells. Data are mean ± SEM from 3 independent experiments. (C-D) Affinity of K1-67 to SORT1. BLI was used to determine the affinity of K1-67 toward human and mouse SORT1 with K1-67 as a ligand and with SORT1-His protein as an analyte. The vertical axis indicates the BLI signal response (nm), and the horizontal line indicates the time after analyte loading. The sensorgram indicates the analyte concentration as follows, dark blue: 100 nM, light blue: 50 nM, red: 25 nM, green: 12.5 nM and yellow: 6.25 nM. Kinetic parameters were analyzed using a 1:1 Langmuir fitting model. Association (K_a) and dissociation (K_d) rate constants were calculated and used to determine the K_D value (K_d/K_a).

Plasma and CSF PGRN up-regulation in K1-67-treated mice

I next tested if down-regulation of SORT1 by anti-SORT1 mAb was able to induce PGRN up-regulation *in vivo*. It is well known that the blood-brain barrier (BBB) prevents the delivery of large molecules, such as proteins or antibodies, to the brain (Pardridge, 2003). To detect PGRN up-regulation, as shown in the mouse primary neuron assay (Fig. 9B), I speculated that K1-67 concentration would need to be more than 1 μg/mL, which would be achieved with a plasma concentration of 200 μg/mL to 1 mg/mL, assuming that the concentration of antibodies in the brain after peripheral treatment is as low as 0.1 to 0.5% of the concentration in the blood (Shin et al., 1995; Pardridge, 2005; Boado et al., 2013). One or three days after a single intravenous administration of K1-67 at 100 mg/kg, plasma concentration of K1-67 reached 570 μg/mL or 460 μg/mL, respectively and there was a trend for an increase in PGRN level in CSF (Fig. 10A to 10C).

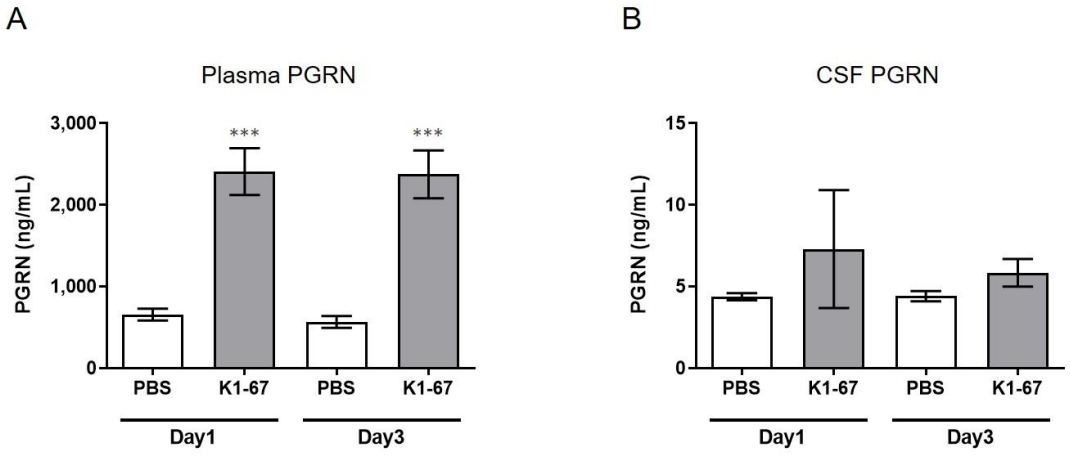

C

K1-67 plasma concentration (μg/mL)

Day	Mean	SD
1	569.7	61.1
3	460.0	52.6

Fig. 10 Up-regulation of plasma or CSF PGRN levels in K1-67-treated mice. (A-B) Plasma or CSF PGRN levels in response to K1-67. Mouse plasma or CSF was collected 1- or 3-days after the treatment of K1-67 at 100 mg/kg, i.v., and subjected to ELISA. Pooled CSF from 4 mouse was used due to the small volume of CSF from individual mouse. The vertical axis indicates PGRN concentration. Data are mean ± SD from 12 or 3-4 independent experiments for plasma and CSF, respectively. ***; $p < 0.001$ vs PBS-treated group by Aspin-Welch t-test. (C) K1-67 concentration in plasma. Mouse plasma was collected 1 or 3 days

after the treatment of K1-67 at 100 mg/kg, i.v., and subjected to liquid chromatography-mass spectrometry. Data are mean ± SD from 3 independent experiments.

Interstitial fluid (ISF) PGRN up-regulation in K1-67-treated mice

In mouse brain, CSF has been reported to be produced at a rate of 350 nL/min, which means the total CSF volume of 40 µL turns over 12-13 times per day (Johanson et al., 2008). This led me to think that the rapid CSF turnover may have influenced the effect of K1-67 on CSF levels and diminished the up-regulation of CSF PGRN levels. Therefore, I considered measuring PGRN levels in the interstitial fluid (ISF), the turnover of which is reportedly lower than that of CSF (Abbott, 2004). To do this I used a microdialysis method, in which ISF could be continuously collected from a probe implanted in the hippocampus and efflux of PGRN could be minimized. I administered K1-67 at two doses of 100 mg/kg, which I speculated was high enough to achieve PGRN up-regulation in the brain, and half of the dose, 50 mg/kg into mice 24 hours prior to the first collection of microdialysates. As shown in Fig. 11, I observed a continuous decline of ISF PGRN levels over time in the PBS-treated group, which I speculate was due to probe membrane clogging by glial cells. Meanwhile, I found significant up-regulation of ISF PGRN levels by K1-67 at after 2 and 4 hours of microdialysate collection (26 and 28 hours after K1-67 treatment, respectively). This result clearly indicated that anti-SORT1 mAb K1-67, boosted ISF PGRN levels in the brain.

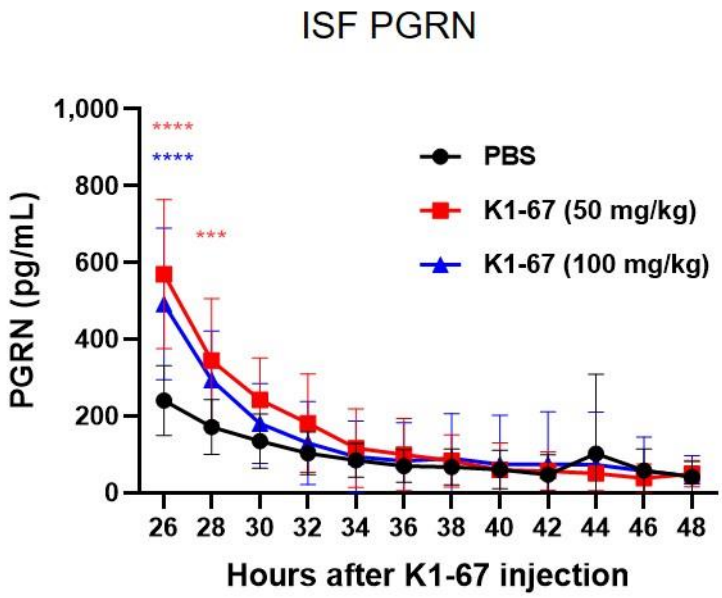

Fig. 11 ISF PGRN levels in response to K1-67. Mouse ISF was collected from a probe in hippocampal microdialysis over 24 hours after the treatment of K1-67 at 50 mg/kg or 100 mg/kg, i.v. PGRN levels were determined by ELISA. The vertical axis indicates PGRN

concentration. The horizontal axis indicates the hours after K1-67 injection. Data are mean ± SD from 10 independent experiments. ***; $p < 0.001$, ****; $p < 0.0001$ vs PBS by Two-way RM ANOVA analysis with Sidak's multiple comparisons.

Discussion

Expected benefits of anti-SORT1 mAb compared with reported PGRN up-regulation

In this study, I demonstrated that SORT1 down-regulation mediated by anti-SORT1 mAb, rather than SORT1-PGRN binding inhibition, led to the up-regulation of PGRN levels. This notion may be useful in exploring SORT1-mediated PGRN up-regulators, as SORT1 is a direct clearance receptor of PGRN. Other compounds, excluding anti-SORT1 mAbs, have been identified to be effective in increasing PGRN levels in cell lines derived from GRN mutation carriers (Capell et al., 2011; Cenik et al., 2011; Holler et al., 2016; Elia et al., 2020). Inhibitors of histone deacetylases (HDACs) was found to increase PGRN gene and protein expression through unknown mechanisms (Cenik et al., 2011). V-ATPase inhibitors enhanced PGRN expression or significantly elevated PGRN secretion via a translational mechanism independent of lysosomal degradation, autophagy, or endocytosis (Capell et al., 2011). Pharmacological inhibition of FOXO1, TRAP1/HSP90L, JMJD6, or ELK3 increased PGRN levels in neurons, inhibiting the activity of their gene products (Elia et al., 2020). Trehalose transcriptionally up-regulates PGRN expression in human and mouse models of GRN haploinsufficiency, and it rescues PGRN deficiency in human fibroblasts and neurons derived from induced pluripotent stem cells generated from *GRN* mutation carriers (Holler et al., 2016). While these drug inhibitors that target genetic modifications of PGRN expression may have potential in treating FTD by up-regulating PGRN, they may produce off-target actions. HDAC inhibitors decrease cell viability at the concentrations that enhance PGRN levels (Cenik et al., 2011). Additionally, none of the abovementioned molecules have been reported to have a PGRN-specific mechanism, unlike SORT1 which is a PGRN clearance receptor. Instead, they act as global regulators of cell functions, such as transcriptional or mitochondrial functions. Previous reports have identified SORT1 binding compounds (Andersen et al., 2014; Schrøder et al., 2014) but their effect on PGRN up-regulation is unknown.

SORT1 down-regulation is a key function to PGRN up-regulation

This study revealed that SORT1 down-regulation activity is essential for up-regulation of PGRN by anti-SORT1 mAb. To date, several therapeutic antibodies have been reported to down-regulate the expression of target proteins (Fan et al., 1994; Chiavenna et al., 2017). The molecular mechanism of antibodies in down-regulation is not fully understood, but it is thought that the binding of the antibody leads to removal of the target protein from the cell surface and alteration of the intracellular fate, resulting in accelerated degradation of the target protein. Considering that SORT1 plays roles in the trafficking of multiple proteins

between the cell surface and lysosome, I assume that anti-SORT1 mAb efficiently uses this property of SORT1 as a protein shuttle to down-regulate itself (Canuel et al., 2008; Hermey, 2009; Musunuru et al., 2010).

Region D in SORT1 is required for PGRN-SORT1 interaction

I discovered several types of anti-SORT1 mAbs which blocked PGRN-SORT1 interaction and/or down-regulated SORT1 down-regulation. A previous report has suggested that PGRN binds to the beta-propeller region of SORT1 through its C-terminal tail (Zheng et al., 2011). Furthermore, another report using HDX-MS technology indicated that PGRN binds to two separate surfaces opposite each other in the cavity of the beta-propeller region of SORT1 and induces conformational dynamics of SORT1 upon binding (Trabjerg et al., 2019). In this study, the mAbs in epitope bins III and VII blocked PGRN-SORT1 interaction and the epitope region of these mAbs was identified as the D region. The beta-propeller region of SORT1 includes the other regions of A, B, and C, suggesting that the D region in SORT1 is the largest contributor to the interaction with PGRN.

Potential therapeutic application in the treatment of FTD

In several studies, plasma and CSF PGRN levels were measured in *GRN* mutant carriers and were found to be significantly lower in FTD patients with *GRN* mutations than in non-mutation carriers, and plasma PGRN was correlated with CSF PGRN in *GRN* mutation carriers (Nicholson et al., 2014). Similarly, low levels of PGRN were observed even in asymptomatic *GRN* mutation carriers (Finch et al., 2009; Galimberti et al., 2018). PGRN levels in *GRN* mutation carriers are 2-3 times lower than in non-mutation carriers and inducing a 2-3 fold increase in PGRN levels could have a therapeutic potential for diseases caused by *GRN* mutation in a haplosufficient manner. In this study, after administration of the anti-SORT1 mAb K1-67, an approximate 2-fold increase in PGRN level was observed in WT mouse brain ISF, demonstrating the potential of anti-SORT1 mAb for increasing PGRN levels. Recently, important roles of PGRN in the lysosome have been discovered and reviewed elsewhere (Paushter et al., 2018). Rare homozygous mutations in *GRN* were shown to cause a juvenile onset lysosomal storage neurodegenerative disorder called neuronal ceroid lipofuscinosis (NCL) (Smith et al, 2012). In agreement with this study, *Grn* KO mice showed lysosomal dysfunction, including lipofuscin deposits and defects in lysosomal turnover (Ahmed et al., 2010; Wils et al., 2012); moreover, FTD patients with *GRN* mutations exhibit lipofuscin deposits in their cortex and retina and fibroblasts derived from these patients have decreased lysosomal protease activity (Ward et al., 2017). Additionally, PGRN is proteolytically processed into GRN peptides in the lysosome (Holler et al., 2017; Zhou et al.,

2017) and both PGRN and GRN levels were found to be reduced in brain lysates from FTD patients with *GRN* mutation (Holler et at. 2017). The authors also revealed that *SORT1* KO HAP1 cells presented increased levels of PGRN and decreased levels of GRN peptides, suggesting that SORT1 plays a role in transporting intracellular PGRN to the lysosome. At the same time, they found that the genetic deletion of *SORT1* did not completely eliminate the production of GRN, which may be controlled by other pathways such as the prosaposin pathway. The anti-SORT1 mAb effect on lysosomal PGRN and GRN peptides may not be the same as that seen in *SORT1* KO cells. However, further studies are needed to validate the effect of anti-SORT1 mAb on intracellular PGRN and GRN peptides and specifically, to demonstrate that anti-SORT1 approach does not reduce the lysosomal pool.

Effect of SORT1 blocking on non-PGRN SORT1 ligands

Several lines of study have emphasized that SORT1 has diverse binding partners, such as pro-forms of NGF and BDNF (Nykjaer et al., 2004; Teng et al., 2005). NGF regulates cell survival and cell death via binding to two different receptors, TrkA and p75NTR (Chao, 2003). In contrast, pro-NGF selectively induces apoptosis through binding to the receptor complex of p75NTR and SORT1. SORT1 is essential for transmitting pro-NGF-dependent death signals via p75NTR (Nykjaer et al., 2004). Similarly, pro-BDNF is an apoptotic ligand that induces death in sympathetic neurons co-expressing SORT1 and p75NTR. The pro-BDNF effect is dependent on cellular co-expression of both p75NTR and SORT1, and competitive antagonists of SORT1 block sympathetic neuron death (Teng et al., 2005). As demonstrated in these reports, the induction of neuron death by pro-NGF or pro-BDNF requires the interaction with SORT1 on the cell surface. Study described here showed that anti-SORT1 mAb up-regulated PGRN levels via SORT1 down-regulation. Potentially, such mAbs remove cell surface SORT1 and would prevent the extracellular interaction of SORT1 to pro-NGF or to pro-BDNF which induce neuron death. Therefore, down-regulation of SORT1 by anti-SORT1 mAbs may have various other beneficial effects than up-regulating PGRN. PGRN is known as an anti-inflammatory factor that stimulates regulatory T-cells through TNF-alpha signal activation (Hu et al., 2014), and administration of PGRN reverses inflammatory arthritis in PGRN-deficient mice models of collagen-induced arthritis (Tang et al., 2011). Up-regulation of PGRN by anti-SORT1 mAb may also be applicable to inflammatory diseases such as arthritis. On the other hand, SORT1 is required for BDNF signaling in neuropathic pain (Richner et al., 2019). In a previous report, polyclonal anti-SORT1 antibody prevented neuropathic pain. The authors also indicated that neurotensin (NTS), one of SORT1 ligands (Mazella et al., 1998), could be involved in the prevention of BDNF signaling-mediated neuropathic pain as AF38469, a small-molecule compound of the NTS binding site of SORT1

(Schrøder et al., 2014), inhibited BDNF-induced neuropathic pain. Removal of cell surface SORT1 by anti-SORT1 mAb may block BDNF signaling and anti-SORT1 mAb may be beneficial for the treatment of neuropathic pain, a major clinical challenge resulting from peripheral nerve trauma or disease.

SORT1 also regulates glucose and lipid metabolism. As observed in *Sort1* KO mice (Devader et al., 2016), NTS levels are expected to be up-regulated by anti-SORT1 antibody with SORT1 down-regulation activity. NTS is involved in a wide variety of biological functions, including glucose homeostasis (Blondeau et al., 2019). The NTS-mediated glucose metabolism is likely mediated through SORT1 as evidenced by the fact that *Nts* KO and *Sort1* KO mice show resistance to obesity and hepatic steatosis, and greater insulin sensitivity on a high fat diet as common phenotypes (Rabinowich et al., 2015; Li et al., 2016). These results suggest that anti-SORT1 mAb might be helpful in maintaining glucose homeostasis by up-regulating NTS. SORT1 was shown to act as an uptake receptor for low-density lipoprotein (LDL) (Strong et al., 2012). They confirmed that plasma LDL is up-regulated in *Sort1* KO mice. While SORT1 also acts as an uptake receptor for very low-density lipoprotein (VLDL, precursor of LDL) (Sparks et al., 2016), it is expected that SORT1 deficiency induces the up-regulation of extracellular VLDL level. However, when SORT1 is genetically knocked-out in mice, VLDL levels are unchanged or reduced, which is inconsistent with a reciprocal relationship (Sparks et al., 2015). This is likely due to the effect of SORT1 on lipoprotein uptake and export (Strong et al., 2014). Therefore, further studies are required to understand the effect of SORT1 down-regulation by anti-SORT1 mAb on lipid metabolism and homeostasis.

In cells, SORT1 acts as a sorting receptor of multiple proteins, including cathepsin D, cathepsin H, GM2AP, prosaposin, and acid sphingomyelinase (Canuel et al., 2009). These proteins use SORT1 to be properly delivered to lysosome and their deficiency causes lysosomal storage disorders. Cathepsin D and acid sphingomyelinase are delivered to lysosomes in both SORT1- and mannose 6-phosphate receptor (MPR)-dependent manner, suggesting that these proteins could be trafficked to lysosomes even when intracellular SORT1 is ablated. However, further research needs to be done to determine if the down-regulation of cell surface SORT1 by anti-SORT1 antibody has an effect on the intracellular sorting function of SORT1 and if lysosomal proteins are properly delivered to lysosomes in the presence of the anti-SORT1 antibody.

Conclusion

I successfully generated a variety of anti-SORT1 antibodies, and identified those that up-regulated PGRN both *in vitro* and *in vivo*. The primary mechanism of PGRN up-regulation was via enhancing SORT1 down-regulation upon antibody binding. This suggests that SORT1 down-regulation is a key mechanism in increasing PGRN levels by anti-SORT1 antibodies and is a promising target for PGRN boosting therapy in disorders such as FTD-PGRN or arthritis, as indicated by *Grn* KO mice phenotype.

General Discussion

In the first part of this study, I succeeded in developing monoclonal antibodies to small-molecule compounds for which antibodies with low antigenicity and high affinity are usually difficult to obtain, even though several state-of-the-art technologies have been developed to generate monoclonal antibodies after development of hybridoma technology. For example, B-cell cloning techniques isolate and clone individual B cells from the immune system of animals or humans exposed to specific antigens (Lin et al., 2020). The cloned B cells are then screened for production of high-affinity antibodies to the antigen of interest, and monoclonal antibodies are obtained by cloning the antibody genes produced. Phage display technology displays antibody fragments on the surface of bacteriophages and screens them for binding to specific antigens (França et al., 2023). This enables rapid generation and selection of high-affinity antibodies against a wide range of targets. Single-cell sequencing technology enables the entire transcriptome of individual cells, including B cells that produce antibodies (Zhu et al., 2023). This helps identify rare or novel antibody sequences that may have unique properties or functions. Synthetic biology involves the design and engineering of novel antibody sequences using computational tools and synthetic biology techniques(Ranjbar et al., 2019). This enables the creation of antibodies with improved properties such as higher affinity, specificity, and stability. These antibody discovery technologies are constantly evolving and improving, and are expected to have a significant impact on the development of new antibodies for scientific research and clinical applications.

Developing antibodies to small molecules can be challenging due to the small size and lack of immunogenicity of these molecules. Small molecules typically do not elicit a strong immune response on their own, so they need to be conjugated to a carrier protein to generate an immune response. Additionally, small molecules often have a low molecular weight and lack complex structures, which can make it difficult to generate antibodies that are specific to the target molecule and do not cross-react with other molecules.

However, this is highly significant in that it shows an example of how specific monoclonal antibodies to small molecules can be produced through technical innovations such as appropriate immunogen design, selection of adaptive experimental methods, and use of the latest technology.

Despite these challenges, antibodies to small molecules can be very useful in a variety of applications. For example, they can be used to detect and quantify small molecules in biological samples, such as blood or tissue. This can be important for understanding the role of small molecules in biological processes and for developing new therapies that target these molecules. Antibodies to small molecules can also be used in diagnostic tests to detect the

presence of small molecules in patient samples, such as in the case of drug monitoring or disease diagnosis.

It is expected to be used in many researches along with specific monoclonal antibodies against small molecules such as ATP, glucose, dopamine, and a few other small molecules. Anti-digoxin antibody: Digoxin is a small molecule drug used to treat heart failure. Anti-digoxin antibodies are used in diagnostic tests to measure the concentration of digoxin in patient blood samples (Chan et al., 2019). In case of anti-cocaine antibody, cocaine is a small molecule drug of abuse. Anti-cocaine antibodies have been developed as a potential therapy for cocaine addiction, as they can bind to cocaine in the bloodstream and prevent it from crossing the blood-brain barrier and producing its psychoactive effects (Stephenson and Toth, 2023). Also, antibodies to steroid hormones have been developed for use in diagnostic tests to measure the concentration of these hormones in patient samples as they play important roles in regulating various physiological processes (Stanczyk et al., 2007). In particular, the cGAMP antibody successfully developed in this study showed high specificity and sensitivity. Therefore, it will be used as a powerful tool to better understand the role of cGAMP in cGAS activation and intracellular signaling, and to assess the involvement of the cGAS-STING pathway in autoimmune diseases and pathologies. Overall, the development of antibodies to small molecules is an important area of research that has the potential to advance the understanding of biology and improve human health.

In the second part of this study, I also generated a monoclonal antibody against SORT1. Then, by examining its binding properties and function in detail, I verified the inhibitory effect of SORT1 function and its mechanism of action, as well as the effect of injection of this antibody *in vivo* in mice on PGRN levels.

Many drugs have been developed as therapeutic antibodies, and their mechanisms are known to include inhibition or activation of signaling pathways, antibody-dependent cytotoxic activity, and drug delivery. The mechanism of action for therapeutic antibodies can vary depending on the specific target and disease being treated. However, in general, therapeutic antibodies work by binding to specific molecules, such as proteins or receptors, and modulating their activity or function. This can include blocking the activity of a molecule, enhancing its activity, or targeting it for destruction by the immune system. For example, Nivolumab and Pembrolizumab are the antibody to PD-1 and they work as immune checkpoint inhibitor by blocking PD-1 and its receptor PD-L1 for treatment of melanoma and other cancers (Patwekar et al., 2023). Aducanumab was developed for Alzheimer's disease treatment, and it reduces beta-amyloid plaques (Gorthi and Gupta, 2023). Anti-CD20 antibody, rituximab, induced antibody dependent cellular cytotoxicity (ADCC) and complement dependent cytotoxicity (CDC) to kill CD20 positive lymphomas (Covic et al.,

2023). Adcetris is one of the antibody-drug conjugate (ADC). Adcetris is internalized with conjugated drug upon binding to CD30 on Hodgkin's lymphoma, and the up-taken drugs efficiently kill the CD30 positive lymphomas (Burton et al., 2023).

To prove the mechanism hypothesis for a therapeutic antibody, several key steps are typically required. Overall, proving the mechanism hypothesis for a therapeutic antibody requires a comprehensive evaluation of the antibody's activity, efficacy, and safety, both *in vitro* and *in vivo*. This is critical to ensure that the antibody is effective and safe for use in humans. This study is significant in that it opens up the possibility of developing antibody drugs with a new mechanism of action that inhibits the binding between the receptor (SORT1) and the ligand (PGRN), thereby increasing the extracellular PGRN concentration. The scientific breakthrough of this study is the discovery that an anti-SORT1 antibody can up-regulate PGRN expression via SORT1 down-regulation in human cells. This finding has important implications for the development of new therapies for neurodegenerative diseases associated with PGRN deficiency, such as frontotemporal dementia (FTD). This novel discovery suggests that targeting SORT1 with an antibody could be a potential therapeutic strategy for FTD and other neurodegenerative diseases associated with PGRN deficiency. This is a significant breakthrough in the field of neurodegenerative disease research and has the potential to lead to the development of new treatments for these devastating disorders.

Through this research, I have successfully demonstrated the possibility of producing monoclonal antibodies specific for low molecular weight compounds and the development of antibody drugs against SORT1. These results are highly valuable in that they have promoted the applied aspects of biology. It is hoped that the results of this research will be the basis for further studies leading to more effective treatments for diseases and a better understanding of disease mechanisms.

Acknowledgements

I am deeply grateful to Professor Kentaro Nakano and Professors Ryusuke Niwa, Ryuhei Harada and Kaori Ishikawa, University of Tsukuba, for guiding my work and valuable discussions through my doctoral program.

I appreciate Drs. Hiroyuki Sakuma, Dnyaneshwar Warude, Satomi Asanuma, Naoto Arimura, Tomoki Yoshihara, Daniel Tavares, Akito Hata, Koh Ida, Yuri Hori, Yuumi Okuzono, Syunsuke Yamamoto, Koichi Iida, Hisao Shimizu, Shinichi Kondo, Toshitake Okui, Tsubasa Shiraishi, Megumi Hirayama, Yoshinori Satomi, Teruki Hamada, Mayumi Nishida and Chihiro Akimoto for valuable suggestions, contributions and helpful supports.

I also greatly appreciate Dr. Shuji Sato for valuable discussion, suggestions and tremendous support.

I also thank Dr. Yusuke Kikukawa, Takeda Pharmaceutical Company Limited, for his understanding and support on my doctoral program.

Finally, I would like to appreciate my family for supporting my life in University of Tsukuba.

References

- Abbott NJ. Evidence for bulk flow of brain interstitial fluid: significance for physiology and pathology. Neurochem Int. 2004 Sep;45(4):545-52. doi: 10.1016/j.neuint.2003.11.006. PMID: 15186921.
- Ablasser A, Goldeck M, Cavlar T, Deimling T, Witte G, Röhl I, Hopfner KP, Ludwig J, Hornung V. cGAS produces a 2'-5'-linked cyclic dinucleotide second messenger that activates STING. Nature. 2013 Jun 20;498(7454):380-4. doi: 10.1038/nature12306. PMID: 23722158.
- Ahmed Z, Sheng H, Xu YF, Lin WL, Innes AE, Gass J, et al. Accelerated lipofuscinosis and ubiquitination in granulin knockout mice suggest a role for progranulin in successful aging. Am J Pathol. 2010;177(1):311-24. doi: 10.2353/ajpath.2010.090915. PMID: 20522652.
- An J, Durcan L, Karr RM, Briggs TA, Rice GI, Teal TH, Woodward JJ, Elkon KB. Expression of Cyclic GMP-AMP Synthase in Patients With Systemic Lupus Erythematosus. Arthritis Rheumatol. 2017 Apr;69(4):800-807. doi: 10.1002/art.40002. PMID: 27863149.
- Andersen JL, Schrøder TJ, Christensen S, Strandbygård D, Pallesen LT, García-Alai MM, et al. Identification of the first small-molecule ligand of the neuronal receptor sortilin and structure determination of the receptor-ligand complex. Acta Crystallogr D Biol Crystallogr. 2014;70(Pt 2):451-460. doi: 10.1107/S1399004713030149. PMID: 24531479.
- Andersson CH, Hansson O, Minthon L, Andreasen N, Blennow K, Zetterberg H, et al. A Genetic Variant of the Sortilin 1 Gene is Associated with Reduced Risk of Alzheimer's Disease. J Alzheimer's Dis. 2016;53(4):1353-1363. doi: 10.3233/JAD-160319. PMID: 27392867.
- Arrant AE, Filiano AJ, Unger DE, Young AH, Roberson ED. Restoring neuronal progranulin reverses deficits in a mouse model of frontotemporal dementia. Brain. 2017;140(5):1447-1465. doi: 10.1093/brain/awx060. PMID: 28379303.
- Benussi L, Ghidoni R, Galimberti D, Boccardi M, Fenoglio C, Scarpini E, et al. The CST3 B haplotype is associated with frontotemporal lobar degeneration. Eur J Neurol. 2010;17(1):143-146. doi: 10.1111/j.1468-1331.2009.02767.x. PMID: 19674067.
- Biilmann, R. L. C. (2016). Antibodies that bind to sortilin and inhibit the binding of progranulin. European Patent Application EP2016/066516. Munich: Germany. European Patent Office.
- Blondeau N, Béraud-Dufour S, Lebrun P, Hivelin C, Coppola T. Sortilin in Glucose

Homeostasis: From Accessory Protein to Key Player? Front Pharmacol. 2019;9:1561. doi: 10.3389/fphar.2018.01561. PMID: 30697159.

- Boado RJ, Hui EK, Lu JZ, Sumbria RK, Pardridge WM. Blood-brain barrier molecular trojan horse enables imaging of brain uptake of radioiodinated recombinant protein in the rhesus monkey. Bioconjug Chem. 2013;24(10):1741-1749. doi: 10.1021/bc400319d. PMID: 24059813.
- Bose D, Su Y, Marcus A, Raulet DH, Hammond MC. An RNA-Based Fluorescent Biosensor for High-Throughput Analysis of the cGAS-cGAMP-STING Pathway. Cell Chem Biol. 2016 Dec 22;23(12):1539-1549. doi: 10.1016/j.chembiol.2016.10.014. PMID: 27889408.
- Burton JS, Foley NC, Mehta-Shah N. SOHO State-of-the-Art Updates and Next Questions: Treatment for Newly Diagnosed Peripheral T-Cell Lymphomas. Clin Lymphoma Myeloma Leuk. 2023 Oct 24:S2152-2650(23)02151-1. doi: 10.1016/j.clml.2023.10.007. PMID: 37973458.
- Canuel M, Korkidakis A, Konnyu K, Morales CR. Sortilin mediates the lysosomal targeting of cathepsins D and H. Biochem Biophys Res Commun. 2008;373(2):292-297. doi: 10.1016/j.bbrc.2008.06.021. PMID: 18559255.
- Canuel M, Libin Y, Morales CR. The interactomics of sortilin: an ancient lysosomal receptor evolving new functions. Histol Histopathol. 2009;24(4):481-492. doi: 10.14670/HH-24.481. PMID: 19224451.
- Capell A, Liebscher S, Fellerer K, Brouwers N, Willem M, Lammich S, et al. Rescue of progranulin deficiency associated with frontotemporal lobar degeneration by alkalizing reagents and inhibition of vacuolar ATPase. J Neurosci. 2011;31(5):1885-1894. doi: 10.1523/JNEUROSCI.5757-10.2011. PMID: 21289198.
- Cenik B, Sephton CF, Dewey CM, Xian X, Wei S, Yu K, et al. Suberoylanilide hydroxamic acid (vorinostat) up-regulates progranulin transcription: rational therapeutic approach to frontotemporal dementia. J Biol Chem. 2011;286(18):16101-16108. doi: 10.1074/jbc.M110.193433. PMID: 21454553.
- Chao MV. Neurotrophins and their receptors: a convergence point for many signalling pathways. Nat Rev Neurosci. 2003;4(4):299-309. doi: 10.1038/nrn1078. PMID: 12671646.
- Chan BS, Isbister GK, Page CB, Isoardi KZ, Chiew AL, Kirby KA, Buckley NA. Clinical outcomes from early use of digoxin-specific antibodies versus observation in chronic digoxin poisoning (ATOM-4). Clin Toxicol (Phila). 2019 Jul;57(7):638-643. doi: 10.1080/15563650.2018.1546010. PMID: 30585517.
- Chiavenna SM, Jaworski JP, Vendrell A. State of the art in anti-cancer mAbs. J Biomed

Sci. 2017;24(1):15. doi: 10.1186/s12929-016-0311-y. PMID: 28219375.

- Civril F, Deimling T, de Oliveira Mann CC, Ablasser A, Moldt M, Witte G, Hornung V, Hopfner KP. Structural mechanism of cytosolic DNA sensing by cGAS. Nature. 2013 Jun 20;498(7454):332-7. doi: 10.1038/nature12305. PMID: 23722159.
- ClinicalTrials.gov. (2020). A Phase 3 Study to Evaluate Efficacy and Safety of AL001 in Frontotemporal Dementia (INFRONT-3). https://clinicaltrials.gov/ct2/show/NCT04374136 [Accessed October 6, 2020].
- Covic A, Caruntu ID, Burlacu A, Giusca SE, Covic A, Stefan AE, Brinza C, Ismail G. Therapeutic Potential of Rituximab in Managing Hepatitis C-Associated Cryoglobulinemic Vasculitis: A Systematic Review. J Clin Med. 2023 Oct 27;12(21):6806. doi: 10.3390/jcm12216806. PMID: 37959271.
- Crow YJ, Manel N. Aicardi-Goutières syndrome and the type I interferonopathies. Nat Rev Immunol. 2015 Jul;15(7):429-40. doi: 10.1038/nri3850. PMID: 26052098.
- Davies BW, Bogard RW, Young TS, Mekalanos JJ. Coordinated regulation of accessory genetic elements produces cyclic di-nucleotides for V. cholerae virulence. Cell. 2012 Apr 13;149(2):358-70. doi: 10.1016/j.cell.2012.01.053. PMID: 22500802.
- Devader C, Moreno S, Roulot M, Deval E, Dix T, Morales CR, et al. Increased Brain Neurotensin and NTSR2 Lead to Weak Nociception in NTSR3/Sortilin Knockout Mice. Front Neurosci. 2016;10:542. doi: 10.3389/fnins.2016.00542. PMID: 27932946.
- Diner EJ, Burdette DL, Wilson SC, Monroe KM, Kellenberger CA, Hyodo M, Hayakawa Y, Hammond MC, Vance RE. The innate immune DNA sensor cGAS produces a noncanonical cyclic dinucleotide that activates human STING. Cell Rep. 2013 May 30;3(5):1355-61. doi: 10.1016/j.celrep.2013.05.009. PMID: 23707065.
- Elia LP, Reisine T, Alijagic A, Finkbeiner S. Approaches to develop therapeutics to treat frontotemporal dementia. Neuropharmacology. 2020;166:107948. doi: 10.1016/j.neuropharm.2020.107948. PMID: 31962288.
- Fan Z, Lu Y, Wu X, Mendelsohn J. Antibody-induced epidermal growth factor receptor dimerization mediates inhibition of autocrine proliferation of A431 squamous carcinoma cells. J Biol Chem. 1994;269(44):27595-27602. PMID: 7961676.
- Finch N, Baker M, Crook R, Swanson K, Kuntz K, Surtees R, et al. Plasma progranulin levels predict progranulin mutation status in frontotemporal dementia patients and asymptomatic family members. Brain. 2009;132(Pt 3):583-591. doi: 10.1093/brain/awn352. PMID: 19158106.
- França RKA, Studart IC, Bezerra MRL, Pontes LQ, Barbosa AMA, Brigido MM, Furtado GP, Maranhão AQ. Progress on Phage Display Technology: Tailoring Antibodies for Cancer Immunotherapy. Viruses. 2023 Sep 9;15(9):1903. doi: 10.3390/v15091903.

PMID: 37766309.

- Galimberti D, Fumagalli GG, Fenoglio C, Cioffi SMG, Arighi A, Serpente M, et al. Progranulin plasma levels predict the presence of GRN mutations in asymptomatic subjects and do not correlate with brain atrophy: results from the GENFI study. Neurobiol Aging. 2018;62:245.e9-245.e12. doi: 10.1016/j.neurobiolaging.2017.10.016. PMID: 29146050.
- Gao D, Li T, Li XD, Chen X, Li QZ, Wight-Carter M, Chen ZJ. Activation of cyclic GMP-AMP synthase by self-DNA causes autoimmune diseases. Proc Natl Acad Sci U S A. 2015 Oct 20;112(42):E5699-705. doi: 10.1073/pnas.1516465112. PMID: 26371324.
- Gao P, Ascano M, Wu Y, Barchet W, Gaffney BL, Zillinger T, Serganov AA, Liu Y, Jones RA, Hartmann G, Tuschl T, Patel DJ. Cyclic [G(2',5')pA(3',5')p] is the metazoan second messenger produced by DNA-activated cyclic GMP-AMP synthase. Cell. 2013 May 23;153(5):1094-107. doi: 10.1016/j.cell.2013.04.046. PMID: 23647843.
- Gentili M, Lahaye X, Nadalin F, Nader GPF, Puig Lombardi E, Herve S, De Silva NS, Rookhuizen DC, Zueva E, Goudot C, Maurin M, Bochnakian A, Amigorena S, Piel M, Fachinetti D, Londoño-Vallejo A, Manel N. The N-Terminal Domain of cGAS Determines Preferential Association with Centromeric DNA and Innate Immune Activation in the Nucleus. Cell Rep. 2019 Feb 26;26(9):2377-2393.e13. doi: 10.1016/j.celrep.2019.01.105. PMID: 30811988.
- Ghidoni R, Benussi L, Glionna M, Franzoni M, Binetti G. Low plasma progranulin levels predict progranulin mutations in frontotemporal lobar degeneration. Neurology. 2008;71(16):1235-1239. doi: 10.1212/01.wnl.0000325058.10218.fc. PMID: 18768919.
- Gorthi SP, Gupta D. Alzheimer's Disease: Treatment Today and Tomorrow. Ann Indian Acad Neurol. 2023 Jul-Aug;26(4):326-333. doi: 10.4103/aian.aian_254_23. PMID: 37970257.
- Gray EE, Treuting PM, Woodward JJ, Stetson DB. Cutting Edge: cGAS Is Required for Lethal Autoimmune Disease in the Trex1-Deficient Mouse Model of Aicardi-Goutières Syndrome. J Immunol. 2015 Sep 1;195(5):1939-43. doi: 10.4049/jimmunol.1500969. PMID: 26223655.
- Hall J, Brault A, Vincent F, Weng S, Wang H, Dumlao D, Aulabaugh A, Aivazian D, Castro D, Chen M, Culp J, Dower K, Gardner J, Hawrylik S, Golenbock D, Hepworth D, Horn M, Jones L, Jones P, Latz E, Li J, Lin LL, Lin W, Lin D, Lovering F, Niljanskul N, Nistler R, Pierce B, Plotnikova O, Schmitt D, Shanker S, Smith J, Snyder W, Subashi T, Trujillo J, Tyminski E, Wang G, Wong J, Lefker B, Dakin L, Leach K. Discovery of PF-06928215 as a high affinity inhibitor of cGAS enabled by a novel fluorescence polarization assay. PLoS One. 2017 Sep 21;12(9):e0184843. doi:

10.1371/journal.pone.0184843. PMID: 28934246.

- Hansen K, Prabakaran T, Laustsen A, Jørgensen SE, Rahbæk SH, Jensen SB, Nielsen R, Leber JH, Decker T, Horan KA, Jakobsen MR, Paludan SR. Listeria monocytogenes induces IFNβ expression through an IFI16-, cGAS- and STING-dependent pathway. EMBO J. 2014 Aug 1;33(15):1654-66. doi: 10.15252/embj.201488029. PMID: 24970844.
- Hanson MG Jr, Shen S, Wiemelt AP, McMorris FA, Barres BA. Cyclic AMP elevation is sufficient to promote the survival of spinal motor neurons in vitro. J Neurosci. 1998 Sep 15;18(18):7361-71. doi: 10.1523/JNEUROSCI.18-18-07361.1998. PMID: 9736656.
- Hashii N, Utoh M, Ohtsu Y, Kato N, Goda R, Goto R, et al. Bioanalytical Quantification of Therapeutic Antibodies by Liquid Chromatography/mass Spectrometry. CHROMATOGRAPHY, 2018;39(1)7-19. doi:10.15583/jpchrom.2017.018.
- Hermey G. The Vps10p-domain receptor family. Cell Mol Life Sci. 2009;66(16):2677-2689. doi: 10.1007/s00018-009-0043-1. PMID: 19434368.
- Holler CJ, Taylor G, Deng Q, Kukar T. Intracellular proteolysis of progranulin generates stable, lysosomal granulins that are haploinsufficient in patients with frontotemporal dementia caused by GRN mutations. eNeuro. 2017;4(4):ENEURO.0100-17.2017. doi: 10.1523/ENEURO.0100-17.2017. PMID: 28828399.
- Holler CJ, Taylor G, McEachin ZT, Deng Q, Watkins WJ, Hudson K, et al. Trehalose upregulates progranulin expression in human and mouse models of GRN haploinsufficiency: a novel therapeutic lead to treat frontotemporal dementia. Mol Neurodegener. 2016;11(1):46. doi: 10.1186/s13024-016-0114-3. PMID: 27341800.
- Hu F, Padukkavidana T, Vægter CB, Brady OA, Zheng Y, Mackenzie IR, et al. Sortilin-mediated endocytosis determines levels of the frontotemporal dementia protein, progranulin. Neuron. 2010;68(4):654-667. doi: 10.1016/j.neuron.2010.09.034. PMID: 21092856.
- Hu Y, Xiao H, Shi T, Oppenheim JJ, Chen X. Progranulin promotes tumour necrosis factor-induced proliferation of suppressive mouse $CD4^+$ $Foxp3^+$ regulatory T cells. Immunology. 2014;142(2):193-201. doi: 10.1111/imm.12241. PMID: 24383743.
- Ishikawa H, Ma Z, Barber GN. STING regulates intracellular DNA-mediated, type I interferon-dependent innate immunity. Nature. 2009 Oct 8;461(7265):788-92. doi: 10.1038/nature08476. PMID: 19776740.
- Johanson CE, Duncan JA III, Klinge PM, Brinker T, Stopa EG, Silverberg GD. Multiplicity of cerebrospinal fluid functions: New challenges in health and disease. Cerebrospinal Fluid Res. 2008;5:10. doi: 10.1186/1743-8454-5-10. PMID: 18479516.
- Kamala T. Hock immunization: a humane alternative to mouse footpad injections. J

Immunol Methods. 2007;328(1-2):204-214. doi: 10.1016/j.jim.2007.08.004. PMID: 17804011.

- Kao AW, McKay A, Singh PP, Brunet A, Huang EJ. Progranulin, lysosomal regulation and neurodegenerative disease. Nat Rev Neurosci. 2017;18(6):325-333. doi: 10.1038/nrn.2017.36. PMID: 28435163.
- Karawajczyk A, Giordanetto F, Benningshof J, Hamza D, Kalliokoski T, Pouwer K, Morgentin R, Nelson A, Müller G, Piechot A, Tzalis D. Expansion of chemical space for collaborative lead generation and drug discovery: the European Lead Factory Perspective. Drug Discov Today. 2015 Nov;20(11):1310-6. doi: 10.1016/j.drudis.2015.09.009. PMID: 26429298.
- Kato K, Ishii R, Goto E, Ishitani R, Tokunaga F, Nureki O. Structural and functional analyses of DNA-sensing and immune activation by human cGAS. PLoS One. 2013 Oct 7;8(10):e76983. doi: 10.1371/journal.pone.0076983. PMID: 24116191.
- Kato Y, Park J, Takamatsu H, Konaka H, Aoki W, Aburaya S, Ueda M, Nishide M, Koyama S, Hayama Y, Kinehara Y, Hirano T, Shima Y, Narazaki M, Kumanogoh A. Apoptosis-derived membrane vesicles drive the cGAS-STING pathway and enhance type I IFN production in systemic lupus erythematosus. Ann Rheum Dis. 2018 Oct;77(10):1507-1515. doi: 10.1136/annrheumdis-2018-212988. PMID: 29945921.
- Köhler G, Milstein C. Continuous cultures of fused cells secreting antibody of predefined specificity. Nature. 1975 Aug 7;256(5517):495-7. doi: 10.1038/256495a0. PMID: 1172191.
- Li J, Song J, Zaytseva YY, Liu Y, Rychahou P, Jiang K, et al. An obligatory role for neurotensin in high-fat-diet-induced obesity. Nature. 2016;533(7603):411-415. doi: 10.1038/nature17662. PMID: 27193687.
- Li X, Shu C, Yi G, Chaton CT, Shelton CL, Diao J, Zuo X, Kao CC, Herr AB, Li P. Cyclic GMP-AMP synthase is activated by double-stranded DNA-induced oligomerization. Immunity. 2013 Dec 12;39(6):1019-31. doi: 10.1016/j.immuni.2013.10.019. PMID: 24332030.
- Li XD, Wu J, Gao D, Wang H, Sun L, Chen ZJ. Pivotal roles of cGAS-cGAMP signaling in antiviral defense and immune adjuvant effects. Science. 2013 Sep 20;341(6152):1390-4. doi: 10.1126/science.1244040. PMID: 23989956; PMCID: PMC3863637.
- Li Y, Li Y, Ye M, Wang D, Zhao J, Sun X, et al. Biological function analysis of monoclonal antibodies against human granulins *in vitro* using U251 cells as a model. Protein Expr Purif. 2017;130:55-62. doi: 10.1016/j.pep.2016.09.019. PMID: 27693922.
- Lin W, Liang WC, Nguy T, Maia M, Tyagi T, Chiu C, Hoi KH, Chen Y, Wu Y. Rapid identification of anti-idiotypic mAbs with high affinity and diverse epitopes by rabbit

single B-cell sorting-culture and cloning technology. PLoS One. 2020 Dec 21;15(12):e0244158. doi: 10.1371/journal.pone.0244158. PMID: 33347473.

- Livingston JH, Crow YJ. Neurologic Phenotypes Associated with Mutations in TREX1, RNASEH2A, RNASEH2B, RNASEH2C, SAMHD1, ADAR1, and IFIH1: Aicardi-Goutières Syndrome and Beyond. Neuropediatrics. 2016 Dec;47(6):355-360. doi: 10.1055/s-0036-1592307. PMID: 27643693.
- Macarron R, Banks MN, Bojanic D, Burns DJ, Cirovic DA, Garyantes T, Green DV, Hertzberg RP, Janzen WP, Paslay JW, Schopfer U, Sittampalam GS. Impact of high-throughput screening in biomedical research. Nat Rev Drug Discov. 2011 Mar;10(3):188-95. doi: 10.1038/nrd3368. PMID: 21358738.
- Martínez M, Hernández AI, Hernanz A. Increased cAMP immunostaining in cerebral vessels in Alzheimer's disease. Brain Res. 2001 Dec 13;922(1):148-52. doi: 10.1016/s0006-8993(01)03009-8. PMID: 11730714.
- Mazella J, Zsürger N, Navarro V, Chabry J, Kaghad M, Caput D, et al. The 100-kDa neurotensin receptor is gp95/sortilin, a non-G-protein-coupled receptor. J Biol Chem. 1998;273(41):26273-26276. doi: 10.1074/jbc.273.41.26273. PMID: 9756851.
- McMillan CT, Toledo JB, Avants BB, Cook PA, Wood EM, Suh E, et al. Genetic and neuroanatomic associations in sporadic frontotemporal lobar degeneration. Neurobiol Aging. 2014;35(6):1473-1482. doi: 10.1016/j.neurobiolaging.2013.11.029. PMID: 24373676.
- Mendsaikhan A, Tooyama I, Walker DG. Microglial Progranulin: Involvement in Alzheimer's Disease and Neurodegenerative Diseases. Cells. 2019;8(3):230. doi: 10.3390/cells8030230. PMID: 30862089.
- Mukherjee O, Wang J, Gitcho M, Chakraverty S, Taylor-Reinwald L, Shears S, et al. Molecular characterization of novel progranulin (GRN) mutations in frontotemporal dementia. Hum Mutat. 2008;29(4):512-521. doi: 10.1002/humu.20681. PMID: 18183624.
- Musunuru K, Strong A, Frank-Kamenetsky M, Lee NE, Ahfeldt T, Sachs KV, Li X, et al. From noncoding variant to phenotype via SORT1 at the 1p13 cholesterol locus. Nature. 2010;466(7307):714-719. doi: 10.1038/nature09266. PMID: 20686566.
- National Research Council (US) Committee for the Update of the Guide for the Care and Use of Laboratory Animals. Guide for the Care and Use of Laboratory Animals. 8th ed. Washington (DC): National Academies Press (US); 2011. PMID: 21595115.
- Ndure J, Flanagan KL. Targeting regulatory T cells to improve vaccine immunogenicity in early life. Front Microbiol. 2014;5:477. doi: 10.3389/fmicb.2014.00477. PMID: 25309517.

- Nicholson AM, Finch NA, Thomas CS, Wojtas A, Rutherford NJ, Mielke MM, et al. Progranulin protein levels are differently regulated in plasma and CSF. Neurology. 2014;82(21):1871-1878. doi: 10.1212/WNL.0000000000000445. PMID: 24771538.
- Nykjaer A, Lee R, Teng KK, Jansen P, Madsen P, Nielsen MS, et al. Sortilin is essential for proNGF-induced neuronal cell death. Nature. 2004;427(6977):843-848. doi: 10.1038/nature02319. PMID: 14985763.
- Paijo J, Döring M, Spanier J, Grabski E, Nooruzzaman M, Schmidt T, Witte G, Messerle M, Hornung V, Kaever V, Kalinke U. cGAS Senses Human Cytomegalovirus and Induces Type I Interferon Responses in Human Monocyte-Derived Cells. PLoS Pathog. 2016 Apr 8;12(4):e1005546. doi: 10.1371/journal.ppat.1005546. PMID: 27058035.
- Pardridge WM. Blood-brain barrier drug targeting: the future of brain drug development. Mol Interv. 2003;3(2):90-105, 51. doi: 10.1124/mi.3.2.90. PMID: 14993430.
- Pardridge WM. The blood-brain barrier: bottleneck in brain drug development. NeuroRx. 2005;2(1):3-14. doi: 10.1602/neurorx.2.1.3. PMID: 15717053.
- Patwekar M, Sehar N, Patwekar F, Medikeri A, Ali S, Aldossri RM, Rehman MU. Novel immune checkpoint targets: A promising therapy for cancer treatments. Int Immunopharmacol. 2023 Nov 16;126:111186. doi: 10.1016/j.intimp.2023.111186. PMID: 37979454.
- Paushter DH, Du H, Feng T, Hu F. The lysosomal function of progranulin, a guardian against neurodegeneration. Acta Neuropathol. 2018;136(1):1-17. doi: 10.1007/s00401-018-1861-8. PMID: 29744576.
- Petersen CM, Nielsen MS, Nykjaer A, Jacobsen L, Tommerup N, Rasmussen HH, et al. Molecular identification of a novel candidate sorting receptor purified from human brain by receptor-associated protein affinity chromatography. J Biol Chem. 1997;272(6):3599-3605. doi: 10.1074/jbc.272.6.3599. PMID: 9013611.
- Philtjens S, Van Mossevelde S, van der Zee J, Wauters E, Dillen L, Vandenbulcke M, et al. Rare nonsynonymous variants in SORT1 are associated with increased risk for frontotemporal dementia. Neurobiol Aging. 2018;66:181.e3-181.e10. doi: 10.1016/j.neurobiolaging.2018.02.011. PMID: 29555433.
- Pottier C, Ravenscroft TA, Sanchez-Contreras M, Rademakers R. Genetics of FTLD: overview and what else we can expect from genetic studies. J Neurochem. 2016;138 Suppl 1:32-53. doi: 10.1111/jnc.13622. PMID: 27009575.
- Quistgaard EM, Grøftehauge MK, Madsen P, Pallesen LT, Christensen B, Sørensen ES, et al. Revisiting the structure of the Vps10 domain of human sortilin and its interaction with neurotensin. Protein Sci. 2014;23(9):1291-1300. doi: 10.1002/pro.2512. PMID: 24985322.

- Rabinowich L, Fishman S, Hubel E, Thurm T, Park WJ, Pewzner-Jung Y, et al. Sortilin deficiency improves the metabolic phenotype and reduces hepatic steatosis of mice subjected to diet-induced obesity. J Hepatol. 2015;62(1):175-181. doi: 10.1016/j.jhep.2014.08.030. PMID: 25173968.
- Rademakers R, Neumann M, Mackenzie IR. Advances in understanding the molecular basis of frontotemporal dementia. Nat Rev Neurol. 2012;8(8):423-434. doi: 10.1038/nrneurol.2012.117. PMID: 22732773.
- Ranjbar MM, Ebrahimi MM, Shahsavandi S, Farhadi T, Mirjalili A, Tebianian M, Motedayen MH. Novel Applications of Immuno-bioinformatics in Vaccine and Bio-product Developments at Research Institutes. Arch Razi Inst. 2019 Sep;74(3):219-233. doi: 10.22092/ari.2018.122523.1224. PMID: 31592587.
- Richner M, Pallesen LT, Ulrichsen M, Poulsen ET, Holm TH, Login H, et al. Sortilin gates neurotensin and BDNF signaling to control peripheral neuropathic pain. Sci Adv. 2019;5(6):eaav9946. doi: 10.1126/sciadv.aav9946. PMID: 31223654.
- Rodero MP, Crow YJ. Type I interferon-mediated monogenic autoinflammation: The type I interferonopathies, a conceptual overview. J Exp Med. 2016 Nov 14;213(12):2527-2538. doi: 10.1084/jem.20161596. PMID: 27821552.
- Schrøder TJ, Christensen S, Lindberg S, Langgård M, David L, Maltas PJ, et al. The identification of AF38469: an orally bioavailable inhibitor of the VPS10P family sorting receptor Sortilin. Bioorg Med Chem Lett. 2014;24(1):177-180. doi: 10.1016/j.bmcl.2013.11.046. PMID: 24355129.
- Sharma S, Campbell AM, Chan J, Schattgen SA, Orlowski GM, Nayar R, Huyler AH, Nündel K, Mohan C, Berg LJ, Shlomchik MJ, Marshak-Rothstein A, Fitzgerald KA. Suppression of systemic autoimmunity by the innate immune adaptor STING. Proc Natl Acad Sci U S A. 2015 Feb 17;112(7):E710-7. doi: 10.1073/pnas.1420217112. PMID: 25646421.
- Shin SU, Friden P, Moran M, Olson T, Kang YS, Pardridge WM, et al. Transferrin-antibody fusion proteins are effective in brain targeting. Proc Natl Acad Sci U S A. 1995;92(7):2820-2824. doi: 10.1073/pnas.92.7.2820. PMID: 7708731.
- Sleegers K, Brouwers N, Van Damme P, Engelborghs S, Gijselinck I, van der Zee J, et al. Serum biomarker for progranulin-associated frontotemporal lobar degeneration. Ann Neurol. 2009;65(5):603-609. doi: 10.1002/ana.21621. PMID: 19288468.
- Sparks CE, Sparks RP, Sparks JD. The enigmatic role of sortilin in lipoprotein metabolism. Curr Opin Lipidol. 2015;26(6):598-600. doi: 10.1097/MOL.0000000000000244. PMID: 26780014.
- Sparks RP, Jenkins JL, Miner GE, Wang Y, Guida WC, Sparks CE, et al.

Phosphatidylinositol (3,4,5)-trisphosphate binds to sortilin and competes with neurotensin: Implications for very low density lipoprotein binding. Biochem Biophys Res Commun. 2016;479(3):551-556. doi: 10.1016/j.bbrc.2016.09.108. PMID: 27666481.

- Stanczyk FZ, Lee JS, Santen RJ. Standardization of steroid hormone assays: why, how, and when? Cancer Epidemiol Biomarkers Prev. 2007 Sep;16(9):1713-9. doi: 10.1158/1055-9965.EPI-06-0765. PMID: 17855686.
- Stephenson RJ, Toth I. Anti-cocaine Vaccine Development: Where Are We Now and Where Are We Going? J Med Chem. 2023 Jun 8;66(11):7086-7100. doi: 10.1021/acs.jmedchem.3c00366. PMID: 37227096.
- Strong A, Ding Q, Edmondson AC, Millar JS, Sachs KV, Li X, et al. Hepatic sortilin regulates both apolipoprotein B secretion and LDL catabolism. J Clin Invest. 2012;122(8):2807-2816. doi: 10.1172/JCI63563. PMID: 22751103.
- Strong A, Patel K, Rader DJ. Sortilin and lipoprotein metabolism: making sense out of complexity. Curr Opin Lipidol. 2014;25(5):350-357. doi: 10.1097/MOL.0000000000000110. PMID: 25101658.
- Sun L, Wu J, Du F, Chen X, Chen ZJ. Cyclic GMP-AMP synthase is a cytosolic DNA sensor that activates the type I interferon pathway. Science. 2013 Feb 15;339(6121):786-91. doi: 10.1126/science.1232458. PMID: 23258413.
- Tanaka Y, Chen ZJ. STING specifies IRF3 phosphorylation by TBK1 in the cytosolic DNA signaling pathway. Sci Signal. 2012 Mar 6;5(214):ra20. doi: 10.1126/scisignal.2002521. PMID: 22394562.
- Tang W, Lu Y, Tian QY, Zhang Y, Guo FJ, Liu GY, et al. The growth factor progranulin binds to TNF receptors and is therapeutic against inflammatory arthritis in mice. Science. 2011;332(6028):478-484. doi: 10.1126/science.1199214. PMID: 21393509.
- Teng HK, Teng KK, Lee R, Wright S, Tevar S, Almeida RD, et al. ProBDNF induces neuronal apoptosis via activation of a receptor complex of p75NTR and sortilin. J Neurosci. 2005;25(22):5455-5463. doi: 10.1523/JNEUROSCI.5123-04.2005. PMID: 15930396.
- Toh H, Chitramuthu BP, Bennett HP, Bateman A. Structure, function, and mechanism of progranulin; the brain and beyond. J Mol Neurosci. 2011;45(3):538-548. doi: 10.1007/s12031-011-9569-4. PMID: 21691802.
- Tönjes A, Scholz M, Krüger J, Krause K, Schleinitz D, Kirsten H, et al. Genome-wide meta-analysis identifies novel determinants of circulating serum progranulin. Hum Mol Genet. 2018;27(3):546-558. doi: 10.1093/hmg/ddx413. PMID: 29186428.
- Trabjerg E, Abu-Asad N, Wan Z, Kartberg F, Christensen S, Rand KD. Investigating the Conformational Response of the Sortilin Receptor upon Binding Endogenous Peptide-

and Protein Ligands by HDX-MS. Structure. 2019;27(7):1103-1113.e3. doi: 10.1016/j.str.2019.04.006. PMID: 31104815.

- Van Damme P, Van Hoecke A, Lambrechts D, Vanacker P, Bogaert E, van Swieten J, et al. Progranulin functions as a neurotrophic factor to regulate neurite outgrowth and enhance neuronal survival. J Cell Biol. 2008;181(1):37-41. doi: 10.1083/jcb.200712039. PMID: 18378771.
- Vincent J, Adura C, Gao P, Luz A, Lama L, Asano Y, Okamoto R, Imaeda T, Aida J, Rothamel K, Gogakos T, Steinberg J, Reasoner S, Aso K, Tuschl T, Patel DJ, Glickman JF, Ascano M. Small molecule inhibition of cGAS reduces interferon expression in primary macrophages from autoimmune mice. Nat Commun. 2017 Sep 29;8(1):750. doi: 10.1038/s41467-017-00833-9. PMID: 28963528.
- Wang Y, Yoshihara T, King S, Le T, Leroy P, Zhao X, et al. Automated High-Throughput Flow Cytometry for High-Content Screening in Antibody Development. SLAS Discov. 2018;23(7):656-666. doi: 10.1177/2472555218776607. PMID: 29898633.
- Ward ME, Chen R, Huang HY, Ludwig C, Telpoukhovskaia M, Taubes A, et al. Individuals with progranulin haploinsufficiency exhibit features of neuronal ceroid lipofuscinosis. Sci Transl Med. 2017;9(385):eaah5642. doi: 10.1126/scitranslmed.aah5642. PMID: 28404863.
- Ward ME, Miller BL. Potential mechanisms of progranulin-deficient FTLD. J Mol Neurosci. 2011;45(3):574-582. doi: 10.1007/s12031-011-9622-3. PMID: 21892758.
- Wiemelt AP, Engleka MJ, Skorupa AF, McMorris FA. Immunochemical visualization and quantitation of cyclic AMP in single cells. J Biol Chem. 1997 Dec 12;272(50):31489-95. doi: 10.1074/jbc.272.50.31489. PMID: 9395484.
- Wils H, Kleinberger G, Pereson S, Janssens J, Capell A, Van Dam D, et al. Cellular ageing, increased mortality and FTLD-TDP-associated neuropathology in progranulin knockout mice. J Pathol. 2012;228(1):67-76. doi: 10.1002/path.4043. PMID: 22733568.
- Wu J, Sun L, Chen X, Du F, Shi H, Chen C, Chen ZJ. Cyclic GMP-AMP is an endogenous second messenger in innate immune signaling by cytosolic DNA. Science. 2013 Feb 15;339(6121):826-30. doi: 10.1126/science.1229963. PMID: 23258412.
- Yamamoto S, Ooshima Y, Nakata M, Yano T, Matsuoka K, Watanabe S, Maeda R, Takahashi H, Takeyama M, Matsumoto Y, Hashimoto T. Generation of gene-targeted mice using embryonic stem cells derived from a transgenic mouse model of Alzheimer's disease. Transgenic Res. 2013 Jun;22(3):537-47. doi: 10.1007/s11248-012-9651-x. PMID: 22961199.
- Yang K, Wang J, Wu M, Li M, Wang Y, Huang X. Mesenchymal stem cells detect and defend against gammaherpesvirus infection via the cGAS-STING pathway. Sci Rep.

2015 Jan 16;5:7820. doi: 10.1038/srep07820. PMID: 25592282.

- Zheng Y, Brady OA, Meng PS, Mao Y, Hu F. C-terminus of progranulin interacts with the beta-propeller region of sortilin to regulate progranulin trafficking. PLoS One. 2011;6(6):e21023. doi: 10.1371/journal.pone.0021023. PMID: 21698296.
- Zhou X, Paushter DH, Feng T, Sun L, Reinheckel T, Hu F. Lysosomal processing of progranulin. Mol Neurodegener. 2017;12(1):62. doi: 10.1186/s13024-017-0205-9. PMID: 28835281.
- Zhu L, Peng Q, Wu Y, Yao X. scBCR-seq revealed a special and novel IG H&L V(D)J allelic inclusion rearrangement and the high proportion dual BCR expressing B cells. Cell Mol Life Sci. 2023 Oct 7;80(11):319. doi: 10.1007/s00018-023-04973-8. PMID: 37804328.